Kinetics of 1 H-13 C multiple-contact cross-polarization as a powerful tool to determine the structure and dynamics of complex materials : application to graphene oxide

Jésus Raya, Alberto Bianco, Jérôme Hirschinger

Kinetics of ^{1}H-^{13}C multiple-contact cross-polarization as a powerful tool to determine the structure and dynamics of complex materials : application to graphene oxide

Jésus Raya [a]*, Alberto Bianco [b] and Jérôme Hirschinger [a]*

[a]Institut de Chimie, UMR 7177 CNRS, Université de Strasbourg, Strasbourg, France
[b]University of Strasbourg, CNRS, Immunology, Immunopathology and Therapeutic Chemistry, UPR 3572, 67000 Strasbourg, France

*Corresponding authors :

hirschinger@unistra.fr

jraya@unistra.fr

Abstract

Hartmann-Hahn cross-polarization (HHCP) is the most widely used solid-state NMR technique to enhance the magnetization of dilute spins from abundant spins. Furthermore, as the kinetics of CP depends on dipolar interactions, it contains valuable information on molecular structure and dynamics. In this work, analytical solutions are derived for the kinetics of HHCP and multiple-contact CP (MC-CP) using both classical and non-classical spin-coupling models including the effects of molecular dynamics and several ^{1}H, ^{13}C relaxation and ^{1}H-^{13}C CP experiments are performed in graphene oxide (GO). HHCP is found to be inefficient in our GO sample due to very fast ^{1}H $T_{1\rho}$ relaxation. By contrast, the MC-CP technique which alleviates most of the magnetization loss by ^{1}H $T_{1\rho}$ relaxation leads to a much larger polarization transfer efficiency reducing the measuring time by an order of magnitude. A detailed analysis of the HHCP and MC-CP kinetics indicates the existence of at least two different kinds of hydroxyl (C-OH) functional groups in GO, the major fraction (~90%) of these groups being in the unusual "slow CP regime" in which the rate of ^{1}H $T_{1\rho}$ relaxation is fast compared to the rate of cross-polarization. This ^{13}C signal component is attributed to mobile C-OH groups interacting preferentially with fast-relaxing water molecules while the remaining carbons (~10%) in the usual "fast CP regime" are assigned to C-OH groups involved in hydrogen bonding with neighboring hydroxyl and/or epoxy groups.

Introduction

Hartmann-Hahn (HH) cross-polarization (CP) combined with magic-angle spinning (MAS) has become a standard technique to obtain high-resolution, high-sensitivity solid-state NMR spectra of dilute spin nuclei (*S*) such as ^{13}C and ^{15}N in the presence of an abundant spin species (*I*), *e.g.*, ^{1}H (1) (2) (3) (4) (5) (6) (7) (8). However, it has been recognized for a long time that CPMAS signal intensities may disagree with the atomic ratios for many reasons (8) (9). One of the major problems arises from the competition between CP and spin-lattice relaxation in the rotating frame. Different chemical groups generally exhibit different CP build-up rates and spin-lattice relaxation times in the rotating frame so that line intensity ratios depend critically on the CP contact time. Hence, in principle, reliable relative peak intensities within a CP spectrum cannot be compared without a careful study of their kinetics of CP by variable-contact-time experiments (8). Methods for obtaining « quantitative » CPMAS spectra have nevertheless been proposed over the past decades (10) (11) (12) (13) (14) (15). Among these techniques, the so-called multiple-contact CP (MC-CP) scheme (16) (17), first discussed by Melchior (18) (19), has been recently shown to provide quantitative ^{13}C NMR spectra of complex organic materials (20) (21) as well as an enhancement of the magnetization transfer when compared to (single-contact) HHCP and adiabatic passage through the HH condition CP (APHH-CP) in static oriented (22) (23) and MAS powder (24) (25) samples. CP also plays a major role for probing short-range ordering and dynamics (8) (26). That is why CP is also commonly applied to the detection of nuclei without an obvious gain in signal intensity. For that it is indispensable to understand the kinetics of the magnetization transfer during CP. The dynamics of this process are well-understood for ^{1}H-^{13}C CP. In most cases, one can find features of two limits of polarization transfer. On the one hand, in systems with relatively weak multiple-spin ^{1}H-^{13}C coupling constants and fast ^{1}H spin-diffusion (SD), CP proceeds exponentially as cross-relaxation and is well accounted for by a spin-temperature approach (4) (27) (28), the so-called classical *I*-*S* model (8). This is typically the case of non-protonated carbons in organic solids. On the other

hand, the presence of strong heteronuclear dipolar interactions, as in the case of protonated carbons, leads to coherent energy transfer (29) (30) (31). The kinetics of CP is then best described by the so-called non-classical *I-I*-S* model (8). Indeed, a number of authors used CP with varying contact time (CPVC) to measure heteronuclear couplings and hence internuclear distances (32) (33) (34) (35) (36) (37) (38). Furthermore, Ernst et al (39) (40) have shown that the *I-S* model should be applied with care even in samples where the build-up of the magnetization can be well approximated by an exponential process.

Graphene oxide (GO), the oxidized form of graphene (41), is currently heavily explored in many technological and medical applications (42) including graphene-based hybrid materials, energy storage, catalysis and many others. However, due to the amorphous and heterogeneous nature of GO, there are still many questions regarding its exact structure (43) (44) (45) (46). MAS NMR spectroscopy appears to be one of the most appropriate analytical technique to elucidate the molecular structure and dynamics of GO. ^{13}C NMR studies of various preparations of GO in the literature show the common feature of signals at ca. 60 ppm (epoxy groups), 70 ppm (hydroxyl groups), and 120-130 ppm (basal graphitic sp^2 carbons) (43) (45) (47) (48) (49). These works validated the structural model proposed by Lerf et al. (43) and demonstrated that epoxide (C-O-C) and C-OH carbons are directly connected.

In this paper, we investigate and analyze in detail the kinetics of ^{1}H-^{13}C HHCP and MC-CP in GO. The experimental results are directly compared with analytical and numerical calculations obtained by using the *I-S* and *I-I*-S* models.

Theoretical considerations

The kinetics of CP experiments are usually treated by a phenomenological theory of spin thermodynamics, the classical *I-S* model (8), which assumes that the rate of the spin diffusion (SD) process among abundant spins is faster than the magnitude of the coupling

interaction between the two spin systems. Although there are a number of objections to the applicability of the *I-S* model in the presence of large heteronuclear interactions and MAS (see below) experimental data can often be accounted for by this approach (8) (28) providing a simple physical picture of the CP dynamics. In the *I-S* model, the *I* and *S* spin systems behave as thermal baths that can be in contact with each other and with the lattice. Under these conditions, the spin-temperature theory can be applied and the rate of polarization transfer between the *I* and *S* spin reservoirs is characterized by a cross-relaxation time T_{IS}. Although the spin-temperature concept is little more than a convenient language when the amplitudes of the radiofrequency (RF) fields applied to the *I* and *S* spins, ω_{1I} and ω_{1S}, are larger than any local dipolar field (spin-lock conditions) its development has led to the establishment of simple equations, which play a similar role for NMR of solids as the Bloch equations do for liquids (50). With these assumptions, the variations of the inverse temperature $\beta = \hbar/kT$ of the *I* and *S* spins in the rotating frame during HHCP, β_I and β_S, are described by a system of first-order differential equations of the following form (4) (8) (27) (28) :

$$\frac{d}{dt}\beta_S(t) = -\frac{1}{T_{IS}}\big(\beta_S(t) - \beta_I(t)\big) - \frac{1}{T_{1\rho}^S}\beta_S(t) \qquad (1)$$

$$\frac{d}{dt}\beta_I(t) = -\frac{\varepsilon}{T_{IS}}\big(\beta_I(t) - \beta_S(t)\big) - \frac{1}{T_{1\rho}^I}\beta_I(t), \qquad (2)$$

where the two last terms account for spin-lattice relaxation in the rotating frame of the *I* and *S* nuclei, governed by the time constants $T_{1\rho}^I$ and $T_{1\rho}^S$, respectively. If the Hartmann-Hahn (HH) condition is fulfilled ($\omega_{1I} = \omega_{1S}$) and both spin species have the same spin quantum number (*e.g.*, ½), the parameter $\varepsilon = (N_S S(S+1)\omega_{1S}^2)/(N_I I(I+1)\omega_{1I}^2)$ (ratio of the heat capacities of the *S* and *I* spins) becomes equal to the spin population ratio N_S/N_I (4) (28). The polarization evolution of the *S*-spin magnetization can be defined as

$$\langle S_z\rangle(t) = \frac{\beta_S(t)}{\beta_{I0}}, \qquad (3)$$

where β_{I0} is the inverse temperature of the *I* spins initially « locked » along the RF field (4). Eq. (3) ensures that the spin polarization is normalized, *i.e.*, $\langle S_z \rangle = 1$ when $\beta_S = \beta_{I0}$ (28). In practice, the relative magnitude (heat capacity) and $T_{1\rho}$ relaxation of an extremely diluted spin bath, such as ^{13}C and ^{15}N, can often be neglected ($\varepsilon = 0$ and $1/T_{1\rho}^S = 0$). The following well-known expression of the polarization of the *S* spins as a function of the contact time is then obtained (refer to Appendix A) (8)

$$\langle S_z \rangle(t_{CP}) = \frac{1}{1 - T_{IS}/T_{1\rho}^I} \left\{ \exp\left(-\frac{t_{CP}}{T_{1\rho}^I}\right) - \exp\left(-\frac{t_{CP}}{T_{IS}}\right) \right\}. \quad (4)$$

Eq. (4) holds whatever the ratio $\lambda_I = T_{IS}/T_{1\rho}^I$. When the usual condition $\lambda_I < 1$ is fulfilled (« fast CP regime »), $\langle S_z \rangle(t_{CP})$ first rises with the time constant $T_{UP} = T_{IS}$, reaches a maximum value $\langle S_z \rangle_{MAX}^{HH} = \lambda_I^{(\lambda_I/(1-\lambda_I))}$ at time $t_{MAX}^{HH} = T_{IS} \ln(\lambda_I)/(\lambda_I - 1)$ (*cf*. Eqs (A.8) and (A.9) in Appendix A) (4) (51), and decreases together with the *I* spin magnetization according to the relaxation time, $T_{DOWN} = T_{1\rho}^I$. On the other hand, in the reverse situation with $\lambda_I > 1$ (« slow CP regime »), it is readily observed that the *S* magnetization rises with $T_{UP} = T_{1\rho}^I$ and decreases with $T_{DOWN} = T_{IS}$. Since Eq. (4) is symmetrical with respect to the interchange of T_{IS} and $T_{1\rho}^I$ it is impossible to determine wether $T_{IS} < T_{1\rho}^I$ or $T_{IS} > T_{1\rho}^I$ from a two-exponential fit of the HHCP dynamics alone. Complementary information from single pulse excitation (SPE), $T_{1\rho}^I$ relaxation or TORQUE (T One Rho QUEnching) experiments (52) is then required (51). Although CP data have already been analyzed under the slow CP assumption (51) (53) (54) (55) Fig. 1(a) shows that HHCP kinetic curves in the case where $T_{IS} \gg T_{1\rho}^I$ may be difficult to record, as $\langle S_z \rangle_{MAX}^{HH} \approx T_{1\rho}^I/T_{IS} \ll 1$ (51). The same features are observed in the general case ($\varepsilon > 0$) (4) although both $\langle S_z \rangle_{MAX}^{HH}$ and t_{MAX}^{HH} decreases with ε when $\lambda_I < 1$ (Fig. 1). Indeed, in the case of negligible $T_{1\rho}^I$ relaxation ($\lambda_I \ll 1$), we have $\langle S_z \rangle(\infty) = 1/(1+\varepsilon)$ so that only half of the initial polarization of the *I* spins can be transferred to the *S* spins when $\varepsilon = 1$. Note also that for small values of λ_I one has to wait a long time compared to T_{IS} for the *S* spin signal to reach its maximum (Fig. 1(b)). However, remember that at least 95% of the maximum signal is reached at $t_{CP} > 3T_{IS}$. On the other hand, $\langle S_z \rangle_{MAX}^{HH}$ and t_{MAX}^{HH} are

found to be independent of ε when $\lambda_I \gg 1$, as $\langle S_z \rangle_{MAX}^{HH} \approx 1/\lambda_I$ and $t_{MAX}^{HH} \approx T_{IS}\ln(\lambda_I)/\lambda_I$ (Fig. 1).

The MC-CP experiment is shown in Fig. 2. After the initial CP step, both the *I* and *S* magnetizations are stored along the static magnetic field $\boldsymbol{B}_0$ by « flip-back » $\pi/2$ pulses. During the mixing time τ_M, the *I* spins involved in the CP transfer repolarize through SD with the remaining *I* spins ($\tau_M \ll T_1^I$) (24) (25) and/or via T_1^I spin-lattice relaxation ($\tau_M > T_1^I$) (10) (20) (21) (22) (23) while the *S* magnetization is retained ($\tau_M \ll T_1^S$). The *I* and *S* magnetizations are returned to the transverse plane and the polarization transfer is repeated again. After N cycles, *i.e.*, $n = N + 1$ CP contacts of duration t_{CP}/n, the free induction decay of the *S* spins is observed. As shown in Appendix A, the variation of the *S*-spin polarization during the MC-CP sequence under the conditions $T_1^I \ll \tau_M \ll T_1^S$ is written ($\varepsilon = 0$ and $1/T_{1\rho}^S = 0$)

$$\langle S_z \rangle (t_{CP} + N\tau_M) = \langle S_z \rangle_{\infty}^{MC} \left(1 - \exp\left(-\frac{t_{CP}}{T_{IS}} \right) \right) \tag{5}$$

with

$$\langle S_z \rangle_{\infty}^{MC} = \frac{\exp\left(-\frac{t_{CP}}{nT_{1\rho}^I} \right) - \exp\left(-\frac{t_{CP}}{nT_{IS}} \right)}{\left(1 - \frac{T_{IS}}{T_{1\rho}^I} \right) \left(1 - \exp\left(-\frac{t_{CP}}{nT_{IS}} \right) \right)}. \tag{6}$$

Eq. (5) demonstrates that T_{IS} can be determined by a *single*-exponential fit of the MC-CP build-up curve since $T_{1\rho}^I$ relaxation only affects the preexponential scaling factor $\langle S_z \rangle_{\infty}^{MC}$. In the slow CP regime, this analysis is clearly superior for measuring T_{IS} compared to fitting standard HHCP curves. Indeed, when the *I* spin relaxation is fast ($\lambda_I > 1$), the exponential term in which T_{IS} is found describes the decay of the CP curve (*cf*. Eq. (4)) and it may difficult to acquire enough reliable points since $\langle S_z \rangle_{MAX}^{HH}$ may be much lower than one (Fig. 1(a)). By contrast, Eq. (6) shows that $\langle S_z \rangle_{\infty}^{MC}$ approaches one when $t_{CP}/n \ll T_{1\rho}^I$. Hence, in principle, it is always possible to make the MC-CP dynamics identical to the one that would be

obtained by HHCP in the absence of $T_{1\rho}$ relaxation of the *I* spins by reducing the duration of the CP steps (Fig. 2). In other words, within the *I-S* model, the MC-CP sequence permits to suppress the $T_{1\rho}^{I}$ dependence of the CP dynamics irrespective of the value of $T_{IS}/T_{1\rho}^{I}$ and one can really speak of $T_{1\rho}^{I}$ relaxation « quenching » by contrast to the *apparent* quenching obtained with the TORQUE experiment only when $T_{IS} \ll T_{1\rho}^{I}$ (51) (52). Indeed, Fig. 3 clearly shows that $\langle S_z \rangle_{\infty}^{MC}$ increases dramatically for all $T_{IS}/T_{1\rho}^{I}$ ratios when t_{CP}/n becomes shorter than $T_{1\rho}^{I}$. Furthermore, this increase is comparatively larger when $T_{IS} > T_{1\rho}^{I}$ (Fig. 3). This fact can be directly deduced from Eq. (6), as

$$\langle S_z \rangle_{\infty}^{MC} \approx \exp\left(-\frac{t_{CP}}{nT_{1\rho}^{I}}\right) \quad \text{when} \quad \lambda_I \ll 1, \tag{7}$$

and

$$\langle S_z \rangle_{\infty}^{MC} \approx \frac{nT_{1\rho}^{I}}{t_{CP}}\left(1 - \exp\left(-\frac{t_{CP}}{nT_{1\rho}^{I}}\right)\right) \quad \text{when} \quad \lambda_I \gg 1. \tag{8}$$

Hence, although the MC-CP technique alleviates in part the intensity distortions introduced by a distribution of T_{IS} values as soon as $t_{CP}/n < \sim T_{1\rho}^{I}$ (compare Figs 1(a) and 3(a)) the method yields quantitative spectra at $t_{CP} > \sim 3T_{IS}$ (provided that $T_{IS} \ll T_{1\rho}^{S}$) only if t_{CP}/n is shorter than $T_{1\rho}^{I}$ by at least an order of magnitude (Fig. 3). On the other hand, MC-CP signals in the fast CP regime ($T_{IS}/T_{1\rho}^{I} < 1$) are observed to be effectively suppressed if $t_{CP}/\left(nT_{1\rho}^{I}\right)$ is larger than ~6 (Fig. 3). The MC-CP technique is then expected to be particularly useful for measuring T_{IS} in the slow CP regime. The extension to the general case ($\varepsilon > 0$) does not change significantly $\langle S_z \rangle_{\infty}^{MC}$ although the time constant of the MC-CP build-up curve T_{IS}^{MC} is generally larger than T_{IS} (Appendix A). In the fast CP regime ($\lambda_I < 1$), the amplitude ratio $r_S = \langle S_z \rangle_{\infty}^{MC}/\langle S_z \rangle_{MAX}^{HH}$ cannot exceed 2.73 ($\varepsilon = 0$) or 3.64 ($\varepsilon = 1$) even if the duration of the CP steps are reduced so that $\langle S_z \rangle_{\infty}^{MC} \approx 1$ ($t_{CP}/n \ll T_{1\rho}^{I}$). As expected, Fig. 4(a and c) shows that much higher $\langle S_z \rangle_{\infty}^{MC}/\langle S_z \rangle_{MAX}^{HH}$ ratios may be obtained in the slow CP regime when $t_{CP}/n < \sim T_{1\rho}^{I}$. Moreover, it is seen that the time ratio $r_T = t_{MAX}^{HH}/T_{IS}^{MC}$ decreases with increasing values of $t_{CP}/(nT_{IS})$ in the fast CP regime when $\varepsilon > 0$ (Fig. 4(b and d)). By contrast, r_T is observed to be independent of $t_{CP}/(nT_{IS})$ when $\lambda_I \gg 1$ ($T_{IS}^{MC} \approx T_{IS}$).

As already mentioned, in principle, the simple *I-S* model of CP dynamics is valid when the SD process accomplished by energy-conserving flip-flop transitions of neighbor *I-I* spin pairs is faster than the magnitude of the coupling interaction between the two spin systems. Indeed, the abundant spin system then behaves as a thermal bath and the spin-temperature concept is valid. This is typically the case of non-protonated carbons in organic solids. On the other hand, the presence of strong heteronuclear interactions, as in the case of protonated carbons, leads to coherent energy transfer causing dipolar oscillations (29) (30) (31). The resulting two-stage character of the polarization transfer for rigid and semi-rigid CH_n groups (n = 1, 2, 3) has been previously observed and analyzed in both static and rotating samples (56) (57) (58). Since oscillations of magnetization between *I* and *S* spins as well as effects of MAS are completely neglected in the spin-temperature approach (59), the applicability of the *I-S* model is questionable. To apprehend the complexity of the spin dynamics calculations, let us treat first the simplest case of an isolated two-spin ½ system. Using the generalized master equation of Zwanzig based on projection-operator and Liouville techniques (60) (61), Marica and Snider (62) have shown that the polarizations of the *S* spin and the *I* spin satisfy the following integro-differential equations for the CP between two ½-spin particles under MAS:

$$\frac{d}{dt}\langle S_z\rangle(t) = -\int_0^t b(t)b(t')[K_{SS}(t-t')\langle S_z\rangle(t') + K_{SI}(t-t')\langle I_z\rangle(t')]dt', \qquad (9)$$

where the *I-S* dipolar coupling is a periodic function of time

$$b(t) = \frac{D_{IS}}{2}\left[\sqrt{2}\sin 2\beta\cos(\gamma + \omega_r t) - \sin^2\beta\cos(2\gamma + 2\omega_r t)\right] \qquad (10)$$

with $D_{IS} = \gamma_I\gamma_S\hbar/r^3$, and the memory kernels are

$$K_{SS}(\tau) = \frac{1}{2}[\cos(\Sigma\tau) + \cos(\Delta\tau)] \qquad (11)$$

$$K_{SI}(\tau) = \frac{1}{2}[\cos(\Sigma\tau) - \cos(\Delta\tau)], \qquad (12)$$

where $\Sigma = \omega_{1I} + \omega_{1S}$ and $\Delta = \omega_{1I} - \omega_{1S}$; the corresponding equation for $\langle I_z\rangle(t)$ is obtained by interchanging *S* and *I* labels on the various terms:

$$\frac{d}{dt}\langle I_z\rangle(t) = -\int_0^t b(t)b(t')[K_{IS}(t-t')\langle S_z\rangle(t') + K_{II}(t-t')\langle I_z\rangle(t')]dt', \qquad (13)$$

where $K_{IS}(\tau) = K_{SI}(\tau)$ and $K_{II}(\tau) = K_{SS}(\tau)$.

Note that Eqs (9) and (13) obtained by using the special properties of ½-spin systems and the special nature of the Hamiltonian are *exact* and valid for *all time* for a pair of ½-spin nuclei (62). However, the derivation of a general analytical solution to Eqs (9) and (13) is difficult due to the time dependence of the *I-S* dipolar coupling (62). A simple analytical expression of the CP dynamics around a sideband matching condition is obtained only under fast MAS conditions ($\omega_r \gg D_{IS}$) (62) (63). Furthermore, in a real situation, the *I-S* spin pair treated above interacts with other spins *I* and will tend to reach thermal equilibrium through SD. Fortunately, because SD is reduced by MAS, the two-spin approximation is expected to become more realistic with increasing spinning speed so that the couplings between abundant spins may be safely neglected.

The calculation of the CP dynamics from first principles becomes practically impossible when considering a multiple-spin system of N_I and N_S spins dipolarly coupled with each others. In this case, the general approach consists in projecting onto selected parts of the Hamiltonian in order to derive kinetic equations as solutions for the thermodynamic coordinates both under static (64) and MAS (65) (66) conditions. Although these Mori type (67) integro-differential equations reveal formal analogies with Eqs (9) and (13) several assumptions and approximations must be made in order to obtain analytical expressions for the kinetic

equations and the CP parameters. Notably, the heteronuclear dipolar coupling Hamiltonian must be small in comparison with the *I* and *S* Zeeman energy reservoirs in the tilted double rotating frame (lowest Born approximation) and the memory kernels are usually assumed to decrease much more rapidly than the thermodynamic coordinates due to the strong homonuclear dipolar coupling among the abundant spins (fast-correlation limit or Markov approximation) (4) (64) (65) (66). Indeed, the fast-correlation assumption permits the calculation of a CP rate constant $1/T_{IS}$ and results in the same pair of coupled differential equations as Eqs (1) and (2) (classical *I*-*S* model) when adding the spin-lattice interaction terms characterising the $T_{1\rho}$ decay of the two spin baths (4). However, as the homonuclear dipolar interactions are averaged by MAS, heteronuclear interactions often lead to coherent energy transfer so that the kinetics of CP has a non-exponential character, *i.e.*, memory (or non-Markovian) effects become important as the kinetic equations involve the history of the system investigated at earlier times (64) (68). It might be possible, though very tedious, to relax the Markov approximation in the memory function approach of Demco and co-workers (4) (64). This would likely result in numerical rather than analytical solutions.

An alternative method is to consider the system as an ensemble of tightly coupled $I^*_{n_I}$- *S* subsystems or clusters (e.g., ^{13}C spins and their n_I directly bonded protons) in thermal contact with a reservoir consisting of all the other *I* spins (29) (30) (31) (58) (69). This is the non-classical *I*-*I**-*S* model (8) (refer to Appendix B) in which spin fluctuations induced by flip-flop transitions within the *I*-spin bath are treated as a relaxation process of the *I** spin(s). In other words, the coupling of the *I**-spin(s) to the infinite reservoir of *I* spins is described by a SD-type superoperator depending on two rate constants, $R_{dp} = 1/T_{dp}$ and $R_{df} = 1/T_{df}$ (58) (69). Generally, it is necessary to resort to rather tedious computations involving exact numerical integration of the quantum mechanical (QM) master equation (Eq. (B.1) in Appendix B) (25). For instance, considering only the Ising term of the *I*-*I** interaction ($R_{df} = 0$) in the case of an *I**-*S* spin pair ($n_I = 1$) and neglecting $T_{1\rho}$ relaxation, the difference and sum expectation values satisfy the following integro-differential equations (70) :

$$\frac{d}{dt}\langle I_z - S_z\rangle(t) = -\int_0^t b(t)b(t')\cos[\Delta(t-t')]\exp\left[-R_{\mathrm{dp}}(t-t')\right]\langle I_z - S_z\rangle(t')dt' \tag{14}$$

$$\frac{d}{dt}\langle I_z + S_z\rangle(t) = -\int_0^t b(t)b(t')\cos[\Sigma(t-t')]\exp\left[-R_{\mathrm{dp}}(t-t')\right]\langle I_z + S_z\rangle(t')dt'. \tag{15}$$

Note that the interaction between the *I** spin and the *I*-spin bath shows up simply by an extra *exponential* decay of rate constant R_{dp} for the memory kernels (*cf*. Eqs (11) and (12)) reflecting the decoherence of the *I*-S* spin system to its multiple-spin environment. Eqs (14) and (15) can be solved exactly only in the static case (no sample spinning) or under fast MAS conditions ($\omega_r \gg D_{IS}$) (70). However, they become identical to Eqs (1) and (2) (classical *I-S* model) with $1/T_{IS} = b^2(0)T_{dp}/2$ and $\varepsilon \equiv \varepsilon^* = N_S/N_I^* = 1/n_I = 1$ (*cf.* Appendix B) with $1/T_{1\rho}^I = 1/T_{1\rho}^S = 0$ in the fast-correlation limit ($D_{IS}T_{dp}$ and $\omega_r T_{dp} \ll 1$), as long as $\Sigma T_{dp} \gg 1$ and $\Delta T_{dp} \ll 1$.

In many applications of the CP technique the influence of thermal mobility on the *I-S* and *I-I* dipolar couplings has to be considered. Random molecular motions cause fluctuations of the spin interactions and, hence, of the local fields. The rate of these fluctuations can be described by a correlation time τ_c. Even in the simplest case of an *I-S* spin pair in two-site exchange, analytical solution for CP under MAS are generally not available and it is necessary to resort to spin dynamics numerical simulations in the intermediate regime ($D_{IS}\tau_c \sim 1$) (71). On the other hand, effects of anisotropic molecular motions are readily calculated in the limit of fast averaging ($D_{IS}\tau_c \ll 1$) as it is accounted for by a reduced (residual) dipolar coupling. In the case of isotropic small-step rotational diffusion, if we assume that the correlation function $\overline{b(t)b(t+\tau)} = (D_{IS}^2/5)\exp(-|\tau|/\tau_c)$ decays with a rate exceeding by far the dipolar coupling ($D_{IS}\tau_c \ll 1$) and the MAS rate ($\omega_r\tau_c \ll 1$) the upper limit of the integral in Eqs (9) and (13) can be taken as infinity because the integrand is negligible for $t \gg \tau_c$. The following equations for the spin polarizations are then obtained :

$$\frac{d}{dt}\langle S_z\rangle(t) = -R_{SS}\langle S_z\rangle(t) - R_{SI}\langle I_z\rangle(t) \qquad (16)$$

$$\frac{d}{dt}\langle I_z\rangle(t) = -R_{IS}\langle S_z\rangle(t) - R_{II}\langle I_z\rangle(t), \qquad (17)$$

where

$$R_{SS} = R_{II} = \frac{D_{IS}^2}{5}\int_0^\infty K_{SS}(\tau)\exp\left(-\frac{\tau}{\tau_c}\right)d\tau = \frac{D_{IS}^2}{10}[J(\Sigma) + J(\Delta)] \qquad (18)$$

$$R_{SI} = R_{IS} = \frac{D_{IS}^2}{5}\int_0^\infty K_{SI}(\tau)\exp\left(-\frac{\tau}{\tau_c}\right)d\tau = \frac{D_{IS}^2}{10}[J(\Sigma) - J(\Delta)]. \qquad (19)$$

The reduced spectral density of thermal motion $J(\omega)$ is provided by the Lorentzian distribution

$$J(\omega) = \frac{\tau_c}{1 + (\omega\tau_c)^2}. \qquad (20)$$

Eqs (16) - (20) are identical to the ones obtained by relaxation theory in the weak-collision case (72) if spectral densities containing the Larmor frequencies are neglected ($\omega_{0I}\tau_c, \omega_{0S}\tau_c \gg 1$). Moreover, when the amplitudes of the applied RF fields are much larger than the rate of the motion ($\Sigma\tau_c \gg 1$) and the Hartmann-Hahn condition is (approximately) satisfied ($\Delta\tau_c \ll 1$), we have $J(\Delta) \gg J(\Sigma)$ so that Eqs (16) and (17) are identical to Eqs (1) and (2) (classical *I*-*S* model) with $1/T_{IS} \approx D_{IS}^2\tau_c/10$ and $\varepsilon = 1$ ($N_I = N_S$ in the case of *I*-*S* spin pairs of 100% abundant nuclei and $1/T_{1\rho}^I = 1/T_{1\rho}^S = 0$). Hence, in this case, the CP dynamics is similar to the one derived from the thermodynamic theory (*I*-*S* model) for which the local field fluctuations are caused by flip-flop transitions within the *I*-spin bath ($\tau_c = \infty$) (4).

The consideration of multiple-spin systems ($n_I > 1$) and random molecular motion greatly complicates the resolution of the QM master equation for the *I*-*I**-*S* model (69) (71).

Appropriate mathematical approximations must then be made. As shown previously (25), analytical solutions to the QM master equation can be conveniently obtained by using the memory function approach (4) (60) (61) (62) (64) (67) (68) and the Anderson-Weiss (AW) approximation (73) (74) (75). Furthermore, since the loss of correlation due to stochastic local-field fluctuations induced by motional and spin exchange are treated on an equal footing this approach is expected to be particularly convenient to describe the combined effects of spin diffusion and molecular motion on CPMAS dynamics. As shown in Appendix B, the *I-I*-S* model is readily extended to the treatment of multiple-spin systems ($n_I > 1$) including molecular dynamics and spin-lattice relaxation. Fig. 5(a and b) compares the *I-I*-S* HHCP and MC-CP dynamics at the $n_{HH} = \pm 1$ HH condition calculated by exact numerical integration of the quantum mechanical master equation with the ones obtained by using the AW theory (Eqs (B.28) and (B.31) in Appendix B). As expected, the AW or Gaussian powder approximation does not account for the transient oscillations following the average time course of the HHCP exact powder calculations (25) (58). A very good agreement between the Gaussian and exact powder calculations is nevertheless observed at short contact times for both the HHCP and MC-CP dynamics (Fig. 5(a and b)). Moreover, since $\sqrt{M_2^{IS}} T_{1\rho}^I, \sqrt{M_2^{IS}} T_{1\rho}^S \geq 44.44$ the decaying slope of the HHCP curve is well approximated by the rate $R_1 = \left(1/T_{1\rho}^I + 1/T_{1\rho}^S\right)/2$ (Eq. (B.26)). A closer inspection of the CP dynamics shows that the MC-CP transfer efficiency is overestimated by the AW model at long contact times if $T_{1\rho}^I = T_{1\rho}^S$, especially when $t_{CP}/n < T_{dp}$ (Fig. 5(a)). This behavior has already been attributed to the fact that all orientational correlations between the CP steps of the MC-CP sequence are neglected in the AW approach (25). By contrast, the *S* spin polarization reached in MC-CP at $t_{CP} > T_{1\rho}^I$ is underestimated by the AW calculation in the case when $1/T_{1\rho}^S = 0$ (Fig. 5(b)). This is not surprising since $T_{1\rho}$ relaxation is exactly accounted for by Eq. (B.25) only if $T_{1\rho}^I = T_{1\rho}^S$. Moreover, because $\sqrt{M_2^{IS}} T_{dp} = 4.44$ the Markov approximation ($\sqrt{M_2^{IS}} T_{dp} \ll 1$) breaks down so that the *I-I*-S* model exhibits memory effects (68). Hence, strictly speaking, the exact numerical MC-CP calculations of Fig. 5(a and b) *cannot* be reproduced by the exponential build-up curve obtained with the AW model (Eq. (B.31)). Indeed, the MC-CP dynamics of Fig. 5(a and b) deviate from an exponential function and are best fitted by two-

exponential curves. However, we have observed that the two resulting T_{IS}^{MC} time constants are close to each other (differing by a factor less than ~ 4) when $t_{CP}/n > T_{dp}$ ($t_{CP}/n =$ 277.5 and 555 μs). This is the reason why these MC-CP exact-powder calculations are relatively well described by Eq. (B.31) when $T_{1\rho}^{I} = T_{1\rho}^{S}$ (Fig. 5(a)).

Since the classical (*I-S*) and non-classical (*I-I*-S*) models converge in the fast-correlation limit ($\sqrt{M_2^{IS}} T_{dp} \ll 1$) with $\varepsilon \equiv \varepsilon^* = N_S/N_I^* = 1/n_I$ (*cf.* Appendix B) we have also reported in Fig. 5(c and d) HHCP and MC-CP dynamics calculations using the spin-temperature concept (Eqs (A.7) and (A.14) in Appendix A). Disregarding the initial non-exponential character and transient oscillations, the HHCP dynamics of the *I-I*-S* model is well approximated by the *I-S* model calculation with $T_{IS} = 0.15$ ms and $\varepsilon = 1$ despite the fact that $\sqrt{M_2^{IS}} T_{dp}$ is as large as 4.44. Furthermore, the MC-CP transfer efficiency at long contact times in the absence of $T_{1\rho}$ relaxation of the *S* spins ($1/T_{1\rho}^{S} = 0$) is well predicted by the simple spin thermodynamics theory (Fig. 5(d)), by contrast with the *I-I*-S* model AW calculation (Fig. 5(b)). This is readily attributed to the fact that $T_{1\rho}$ relaxation is exactly treated in the classical *I-S* model (*cf*. Appendix A). On the other hand, the short-time behavior of the MC-CP dynamics of the *I-I*-S* and *I-S* models depart significantly from each other when $t_{CP}/n < T_{IS}$. While the MC-CP build-up rate of the classical (*I-S*) calculation increases steadily towards $1/T_{IS}$ when decreasing t_{CP}/n this is not the case of the non-classical (*I-I*-S*) model calculations at $t_{CP}/n =$ 50 and 138.8 μs due to non-Markovian behavior. Indeed, within the *I-I*-S* model, the MC-CP rate goes to zero as $t_{CP}/n \to 0$. This fact is found to be reminiscent of the Gaussian short-time behavior of the HHCP dynamics (8) (58) (68) which cannot be neglected since T_{dp} is quite long. Fig. 5(c and d) nevertheless shows that the numerical calculations are well described by the *I-S* model when $t_{CP}/n > T_{IS}$ ($t_{CP}/n =$ 277.5 and 555 μs): whereas Eqs (A.14) and (B.31) yield identical results when $T_{1\rho}^{I} = T_{1\rho}^{S}$ (Fig. 5(a and c)) the *I-S* model provides a better agreement with the exact-powder calculations than the AW approximation in the absence of $T_{1\rho}^{S}$ relaxation (Fig. 5(b and d)). We have evaluated the range of validity of the simplified thermodynamic (*I-S*) and AW (*I-I*-S*) analytical solutions by comparison with exact numerical integration of the QM master equation in the usual case where the

condition $T_{IS} \ll T_{1\rho}^{I}$is fulfilled (fast CP regime). However, the reverse situation $T_{IS} \gg T_{1\rho}^{I}$ (slow CP regime) which is likely to occur in the presence of molecular motion with $\tau_c \sim 1/\omega_{1I}$ must also be considered.

As expected, the AW calculations of Fig. 6(a) show that molecular motion has a profound effect on the HHCP build-up rate in the intermediate regime (0.1 ms > τ_c > 1 μs) in agreement with previous works (68) (71). The polarization transfer becomes less efficient and, in the case of a fast anisotropic motion, the HHCP dynamics depends on the averaged interaction through the reduced second moment $S^2 M_2^{IS}$ ($0 < S^2 < 1$). Furthermore, Fig. 6(b) shows that the AW HHCP build-up curve in the fast-averaging limit with $S^2 = 0.1$ is close to an exponential function with $T_{IS} = 1.3$ ms ($|S|\sqrt{M_2^{IS}} T_{dp} < 1$) and agrees well at short contact times with an exact-powder calculation with a reduced effective (residual) *I*-S* dipolar coupling. As previously mentioned, when τ_c is comparable to $1/\omega_{1I}$ (and $1/\omega_{1S}$) the CP kinetics must also be strongly affected by rotating-frame spin-lattice relaxation (*cf*. Appendix B). The HHCP and MC-CP dynamics of the *I-I*-S* and *I-S* models in the presence of fast $T_{1\rho}$ relaxation of the *I* spins ($T_{1\rho}^{I} = 0.1$ ms) are compared in Fig. 6(b). The good agreement obtained confirms that the simple analytical solutions of the *I-S* model may be used as an alternative to exact numerical computations to obtain the kinetic parameters.

Experimental section

The GO sample was provided by Grupo Antolin (Spain). This GO was obtained from carbon nanofibers. These fibers are made of ribbons of about five graphene layers. They are reduced in their length and exfoliated to form GO under strong acid conditions. The presence of adsorbed water molecules was previoulsly assessed using TGA and FT-IR (47). The TGA curve displayed a weight loss of around 13% below 150°C. The presence of water molecules was also observed in the FT-IR spectrum (47), although infrared spectroscopy does not allow to determine its amount. This GO consists of a fine powder that was directly used to fill the NMR rotor without any grinding process.

All the NMR experiments applied to GO were performed at room temperature on a Bruker Avance III 750 spectrometer, operating at frequencies of 188.65 and 750.19 MHz for ^{13}C and ^{1}H resonance, respectively, and equipped with a Bruker triple resonance MAS probe using 3.2-mm-o.d. zirconia rotors. The spinning frequency was fixed at $\nu_r = 18$ kHz. CP and SPE ^{13}C MAS spectra of GO were acquired with a recycle time of 1 s and 30 s, respectively. Proton decoupling during acquisition was obtained by using SPINAL-64 (76). The HHCP and MC-CP ^{1}H-^{13}C dynamics in GO were recorded with the proton and carbon RF fields adjusted to fulfill the first-order sideband ($n_{HH} = 1$) HH condition at $\omega_{1H}/2\pi = 72.2$ kHz and $\omega_{1C}/2\pi = 54.2$ kHz. Independent and direct measurements of the ^{1}H and ^{13}C spin-lattice relaxation times in the laboratory (T_1) and rotating frame ($T_{1\rho}$) have also been performed (*cf*. ESI Sections 2 and 3). The inversion-recovery (IR) $\pi - t_{IR} - \pi/2$ pulse sequence was used to obtain T_1 in ^{1}H and ^{13}C resonance. A spin-lock (SL) sequence consisting of an initial $\pi/2$ pulse followed by a long 90° phase shifted pulse of duration t_{SL} was employed for the ^{1}H and ^{13}C $T_{1\rho}$ relaxation measurements. The T_1 and $T_{1\rho}$ relaxation times were obtained by fitting the line intensity as a function of t_{IR} and t_{SL}, respectively, to a sum of exponentials (*cf*. ESI Figs S2-S5). In both the CP, SPE, IR and SL experiments, an additional rotor-synchronized refocusing pulse has been included after a delay $\tau = T_r$ (55.55 μs) or $6T_r$ (333.33 μs) prior to acquisition in order to reduce spectral distortions (77) (78). HHCP and MC-CP dynamics were simulated by using the analytical expressions given in the theoretical section or by integrating numerically the QM master equation, Eq. (B.1), as described previously (57) (58).

Results and discussion

Various solid-state ^{13}C and ^{1}H NMR experiments were performed on our GO sample (see Figs 7, 8 and ESI Figs S1-S6). Fig. 7 compares the quantitative SPE ^{13}C spectrum of GO with the one obtained by HHCP ($t_{CP} = 555\ \mu s$). Although the observed chemical shifts are in good agreement with previously reported data (47) the HHCP peak intensities strongly disagree with the atomic ratios. Moreover, no improvement of the signal-to-noise ratio is achieved by

the HHCP technique (Fig. 7). These observations are readily attributed to the competition between CP and $T_{1\rho}$ relaxation of the ^{1}H nuclei ($T_{1\rho}^{H}$) (8) (51). As known, the main sources of ^{1}H nuclear polarization for ^{13}C in CPMAS experiments of GO are the hydroxyl (C-OH) groups and water molecules bound to the surface and those entrapped/intercalated between the GO sheets (43). In the usual assumption that $T_{CH} < T_{1\rho}^{H}$ (fast CP regime), Fig. 8(a) shows that the average CP build-up rate $1/T_{CH}$ of the carbon atoms of the C-OH groups is higher than the one of the epoxy (C-O-C) groups. Therefore, signal intensities will not be comparable in short-contact-time CP (SCT-CP) spectra ($t_{CP} < \sim$0.5 ms). Actually, in heterogeneous and proton deficient systems like GO, only long CP contact times of several milliseconds could possibly permit a complete transfer of magnetization to all ^{13}C sites ($t_{CP} \gg T_{IS}$ for all ^{13}C resonances) (10) (11). Unfortunately, reliable HHCP peak intensities are not observable in GO due to fast $T_{1\rho}^{H}$ relaxation (Fig. 8(a)). Indeed, the HHCP intensity for the C-OH, C-O-C and sp^2-bonded (C=C) carbon atoms rapidly decreases after a maximum located at $t_{MAX}^{HH} \approx$ 0.25, 0.8 and 0.6 ms, respectively. Fig. 8(b) demonstrates that the MC-CP technique which alleviates most of the magnetization loss due to $T_{1\rho}^{H}$ relaxation leads to a much larger polarization transfer efficiency : the steady state polarization reached for MC-CP yields a signal enhancement relative to the maximum value obtained in HHCP by a factor ($\langle S_z \rangle_{\infty}^{MC} / \langle S_z \rangle_{MAX}^{HH}$) of 2.8, 2.5 and 2 at the C-OH, C-O-C and C=C resonances, respectively (Fig. 8). However, by contrast with recent MC-CP results in complex organic materials (20) (79), line intensity distortions introduced by the distribution of CP rates and $T_{1\rho}^{H}$ values are not significantly diminished in GO because the C-O-C and C=C carbons still are weakly cross-polarized at a contact time of ~ 7 ms (Fig. 8(b)), as in the SCT-CP spectrum of Fig. 7 ($t_{CP} = 555\ \mu s$). The reason is that in GO many epoxy and *sp*^{2} carbons situated within aromatic clusters are characterized by much weaker CP rates than the C-OH carbons. The accumulation of ^{13}C magnetization by MC-CP then requires a prohibitively long total contact time ($t_{CP} > T_{CH}$) and is hampered by $T_{1\rho}^{C}$ relaxation, as the *S* spin polarization is scaled down by a factor $\left(1 + T_{CH}/T_{1\rho}^{C}\right)^{-1}$ (8).

Our ^{1}H and ^{13}C T_1 relaxation study of GO (see ESI Section 2) shows that the condition $T_1^H \ll \tau_M \ll T_1^C$ is satisfied for the relevant spectral lines in the case of the MC-CP experiments of Fig. 8(b) ($\tau_M = 50$ ms). Assuming that the phenomenological spin-temperature approach with $\varepsilon = 0$ is valid (the natural abundance of ^{13}C is 1%), the MC-CP build-up in a homogeneous system should then be an exponential curve of time constant $T_{CH}^{MC} = T_{CH}$ (*cf.* theoretical section and Appendix A). By contrast, the experimental MC-CP data with $t_{CP}/n = 277.5$ μs at 70 ppm (C-OH resonance) exhibit two exponential components (ESI Fig. S6) with time constants : $T_{CH}^{MC(1)} = 0.25$ ms (36%) and $T_{CH}^{MC(2)} = 1.1$ ms (64%). A separation into two components is outside of experimental accuracy for the MC-CP kinetics at the C-O-C (59 ppm) and C=C (129 ppm) low intensity lines (Fig. 8(b)). The analysis presented below is then restricted to the dominant CP signal at the C-OH sites (70 ppm). The two-exponential MC-CP build-up may be readily attributed to the heterogeneous nature of our system. However, the two time constants $T_{CH}^{MC(1)}$ and $T_{CH}^{MC(2)}$ differing only by a factor ~4, a non-exponential behavior due to the breaking down of the Markov approximation cannot be excluded (*cf*. Fig. 5). Indeed, the rapid increase of the ^{13}C magnetization at the C-OH sites during HHCP (Fig. 8(a)) is consistent with the presence of large ^{13}C-^{1}H interactions although no dipolar oscillations are detected. In order to rule out memory effects, let us first assume that our system is well approximated by a single value for the CP time constant T_{CH}. If the usual $T_{CH} < T_{1\rho}^H$ situation holds (fast CP regime) the C-OH HHCP dynamics of Fig. 8(a) is well fitted with $T_{UP} = T_{CH} \approx 0.1$ ms and $T_{DOWN} = T_{1\rho}^H \approx 2$ ms ($\varepsilon = 0$), *i.e.*, $\lambda_H = T_{CH}/T_{1\rho}^H \approx 0.05$. Using this value of λ_H together with $t_{CP}/(nT_{CH}) \approx 2.8$, Fig. 4(a and b) shows that $r_S = \langle S_z \rangle_\infty^{MC}/\langle S_z \rangle_{MAX}^{HH} \approx 1$ and $r_T = t_{MAX}^{HH}/T_{CH}^{MC} \approx 3$. These results clearly disagree with the experimental data of Fig. 8 : $r_S \approx 2.8$ and $r_T \approx 0.4$. Note however that relaxing the simplified constraint $\varepsilon = 0$ improves significantly the agreement with experiment since Fig. 4(c and d) leads to $r_S \approx 2$ and $r_T \approx 0.6$ for $\varepsilon = 1$. As suggested by the calculations of Fig. 5, this may be attributed to the fact that the *I-I*-S* model better describes the CP results ($\varepsilon \equiv \varepsilon^*$). In the opposite case (slow CP regime), *i.e.*, $T_{UP} = T_{1\rho}^H \approx 0.1$ ms and $T_{DOWN} = T_{CH} \approx 2$ ms ($\lambda_H \approx 20$), Fig. 4 leads to a much higher r_S ratio (~8) and a lower value of r_T (~0.2) irrespective of ε that also do not account for the experimental results. The presence of large amount of C-

OH carbons coupled to protons under the condition $T_{CH} \gg T_{1\rho}^{H}$ is nevertheless consistent with the fact that $\langle S_z \rangle_{\infty}^{MC}$ is reduced by a factor 1.8 when t_{CP}/n is increased from 277.5 μs to 555 μs (Fig. 8(b)). Indeed, Fig. 3(b) shows that such a behavior is characteristic of the slow CP regime as long as the CP steps of the MC-CP sequence are longer that twice the $T_{1\rho}$ relaxation time of the proton spins ($t_{CP}/\left(nT_{1\rho}^{H}\right) > \sim 2$). This condition is clearly fulfilled if $T_{1\rho}^{H} \approx$ 0.1 ms. By contrast, in the case of the fast CP regime ($T_{DOWN} = T_{1\rho}^{H} \approx$ 2 ms), doubling the length of the CP steps can only lead to a marginal change of $\langle S_z \rangle_{\infty}^{MC}$ (10% decrease whatever the value of ε) since $t_{CP}/\left(nT_{1\rho}^{H}\right)$ then varies from ~0.14 to ~0.28 (Fig. 3(b)). It is then concluded that a simple model in which the C-OH groups are characterized by a single value of T_{CH} and/or $T_{1\rho}^{H}$ is inadequate for GO. In accordance with both the T_1 and $T_{1\rho}$ relaxation results (ESI Sections 2 and 3), this two-exponential behavior implies that two (or more) different carbon and proton environments must be considered in GO although a single isotropic C-OH resonance signal is observed (Fig. 7). Indeed, it is well established that non-exponential CP build-up and/or $T_{1\rho}^{H}$ spin-lattice relaxation can arise from the presence of different phases or sites within the same phase, reflecting for instance motional disorder (5) (6) (51) (53) (54) (80) (81). We shall assume here, as it is generally done, that the relaxation time $T_{1\rho}^{H}$ is the same during the spin lock and CP periods. ^{1}H $T_{1\rho}$ relaxation decays with spin-echo delay values $\tau =$ 55.55 μs (one rotor period) and $\tau =$ 333.33 μs (six rotor periods) both are well described by two-exponential curves with a short (fast-relaxing) ill-defined component, $T_{1\rho S}^{H} \sim$ 0.05 - 0.3 ms, and a long (slow-relaxing) component, $T_{1\rho L}^{H} \approx$ 2 ms (ESI Fig. S4). The observed HHCP build-up constant $T_{UP} \approx$ 0.1 ms (Fig. 8(a)) may then be ascribed to $T_{1\rho S}^{H}$ (slow CP regime). Note that rapidly relaxing water molecules with $T_{1\rho}^{H}(\mathrm{H_2O})$ ranging from 0.4 to 0.8 ms have been previously observed in several hydrous silicates (51) (53) (54). By contrast to direct ^{1}H $T_{1\rho}$ relaxation measurements using a Hahn-echo refocusing pulse, the HHCP and MC-CP data are not affected by T_2^H relaxation (the whole ^{1}H magnetization is initially spin-locked) and no significant loss of ^{13}C magnetization is observed before signal acquisition ($\tau =$ 55.55 μs and $T_2^C \gg T_2^H$). The ^{13}C relaxation measurements show that $T_{1\rho}^{C} \gtrsim$ 7 - 9 ms for all chemical sites (ESI Fig. S5). Neglecting $T_{1\rho}^{C}$ relaxation ($T_{1\rho}^{C} \gg T_{1\rho L}^{H}$) and assuming that $\varepsilon = 0$, the four parameters $T_{CH}^{MC(1)} = T_{CH}^{(1)} =$ 0.25 ms,

$T_{CH}^{MC(2)} = T_{CH}^{(2)} = 1$ ms, $T_{1\rho S}^{H} = 0.1$ ms and $T_{1\rho L}^{H} = 2$ ms that are consistent with both the MC-CP and $T_{1\rho}^{H}$ relaxation experiments must be assigned to the two components of our system in order to obtain the couplings between the ^{1}H and ^{13}C spin reservoirs and to the lattice. This can be done by model calculations of the HHCP and MC-CP dynamics (*cf*. theoretical section). Assuming that the CP kinetics follows the *I-S* model, it is remarked that the fraction of each component can always be adjusted so that all possible assignments give a perfect agreement with the MC-CP data. The simulations of the HHCP and MC-CP ($t_{CP}/n = 277.5$ μs) corresponding to all possible cases are compared with the experimental data in Fig. 9. In Fig. 9(a) (case 1), both components are considered to relax with $T_{1\rho L}^{H}$ ($T_{1\rho}^{H(1)} = T_{1\rho}^{H(2)} = 2$ ms), *i.e.*, $T_{1\rho}$ relaxation of the hydroxyl protons does not depend on the C-OH carbon species involved. This would be the case if the ^{13}C spins are not at all cross-polarized by the fast relaxing ^{1}H spins (*e.g.*, mobile protons of bulk water (82)). This first case can clearly be excluded because the experimental values of both $\langle S_z \rangle_{MAX}^{HH}$ and t_{MAX}^{HH} are found to be largely overestimated by the calculation (Fig. 9(a)). A much better agreement is obtained when considering that the major fraction (83%) of the C-OH groups are in the slow CP regime (case 2) (Fig. 9(c)). The HHCP and MC-CP curves are then interpreted as composed of two types of hydroxyl sites having dramatically different abilities to cross polarize (Fig. 9(d)). In quantitative terms, the results of Figs 9(c) and 9(d) show that when a dominant population of carbons is in the slow CP regime, even a small fraction of carbons within the fast CP regime may increase to a significant extent $\langle S \rangle_{MAX}^{HH}$. Moreover, this would correspond to a more realistic situation where a majority of motionally disordered C-OH groups with $T_{CH} \gg T_{1\rho}^{H}$ coexist with a minor fraction of rigid C-OH groups with $T_{CH} \ll T_{1\rho}^{H}$. By contrast, Fig. 9(e) shows that the « unphysical » opposite case (case 3) where the $T_{CH}^{(1)}$ and $T_{CH}^{(2)}$ CP time constants are associated with the $T_{1\rho S}^{H}$ and $T_{1\rho L}^{H}$ relaxation times, respectively, gives a poor agreement with the HHCP experiment. For completeness, we have checked that the highly unprobable solution where all ^{13}C spins are cross-polarized by fast relaxing protons with $T_{1\rho}^{H} = 0.1$ ms (case 4) must also be excluded (Fig. 9(g)). In conclusion, the assignment of Fig. 9(c) clearly provides the best agreement with both the HHCP, MC-CP and relaxation data in GO. However, a close inspection of Fig. 9(c) shows that the experimental HHCP dynamics still

reaches its maximum earlier and at a lower level than the simulation. This discrepancy may be attributed to the fact that the rigid component ($T_{CH}^{(1)} = 0.25$ ms ; $T_{1\rho}^{H(1)} = 2$ ms) does not comply with the classical kinetic model. Indeed, for rigid and fairly isolated C-OH groups, the timescale of the polarization transfer becomes comparable to the spin diffusion rate and the fast-correlation limit or Markov approximation is no longer valid. As already mentioned, memory effects are present and CP is better described by the non-classical *I-I*-S* model (Appendix B). In the theoretical section, we have demonstrated that the *I-I*-S* model can be conveniently approximated by the classical *I-S* model with $\varepsilon \equiv \varepsilon^* = 1/n_I$ as long as the duration of the MC-CP contacts is longer than the CP time constant ($t_{CP}/n > T_{IS}$). We expect this condition to be verified in experiments with $t_{CP}/n > 0.25$ ms (*cf.* theoretical section). Fig. 10 then shows that the *I-S* model with $\varepsilon^{(1)} = 0.5$ ($n_I = 2$) permits to remove all discrepancies observed in Fig. 9(c) and gives an excellent agreement with the additional MC-CP experiment at $t_{CP}/n = 555$ µs. This is a consequence of the increase of the amplitude ration $r_S^{(1)}$ and the decrease of the time ratio $r_T^{(1)}$ due to the fact that $\varepsilon^{(1)} > 0$ (*cf.* Fig. 4). These results fit well with a bottleneck situation where CP at short contact times in the rigid C-OH units ($T_{CH} \approx 0.1$ ms) is limited by spin diffusion to their nearest neighboring protons ($n_I \sim 1$). As expected, the equilibrium polarizations calculated from the MC-CP data with $t_{CP}/n = 277.5$ µs and 555 µs, $\langle S \rangle_\infty^{MC} = 0.377$ and 0.213 (Fig. 10(a)), are much lower than one, the optimum value reached when $t_{CP}/n \ll T_{1\rho}^I$ (*cf.* Fig. 3). Fig. 10(b) also shows that the large decrease in the MC-CP signal intensity observed when increasing t_{CP}/n from 277.5 to 555 µs is almost exclusively accounted for by the fast relaxing component. This result clearly confirms that the major fraction of the C-OH carbons is in the slow CP regime. Indeed, Fig. 3(a) demonstrates that only a small decrease of $\langle S \rangle_\infty^{MC}$ (~10%) is possible irrespective of the value of $T_{CH}/T_{1\rho}^H$ when $T_{1\rho}^H = 2$ ms, *i.e.*, $t_{CP}/\left(nT_{1\rho}^H\right)$ varies from 0.14 to 0.28. By contrast, the reduction of $\langle S \rangle_\infty^{MC}$ by a factor ~2 (from 0.32 to 0.15) agrees well with calculated values for $T_{CH}/T_{1\rho}^H \gg 1$ at $t_{CP}/\left(nT_{1\rho}^H\right) = 2.78$ and 5.55 corresponding to $T_{1\rho}^H = 0.1$ ms (*cf.* Fig. 3(b)). Finally, we have checked that the ^{1}H-^{13}C CPMAS dynamics cannot be accounted for by a single-component fit. Indeed, although the slow CP regime assumption provides a reasonable agreement with the steady state polarizations reached for MC-CP

relative to the maximum value obtained in HHCP ($\langle S_z\rangle_\infty^{MC}/\langle S_z\rangle_{MAX}^{HH}$) it gives a poor agreement with the HHCP experiment at long contact times (Fig. 10(c)). Moreover, as expected (*cf*. ESI Fig. S6), the MC-CP data depart significantly from the calculated (exponential) build-up curves.

In summary, our results strongly suggest the presence of two types of C-OH groups in GO with different mobility. The major component (~90%) in the slow CP regime is attributed to mobile C-OH groups interacting with fast-relaxing water molecules ($T_{IS}^{(2)} \approx$ 1 ms ; $T_{1\rho}^{H(2)} \approx$ 0.1 ms ; $\varepsilon \approx 0$) while the remaining carbons (~10%) in the fast CP regime interact strongly with hydroxyl protons involved in hydrogen bonding with neighboring hydroxy and/or epoxy groups (83) ($T_{IS}^{(1)} \approx$ 0.1 ms ; $T_{1\rho}^{H(1)} \approx$ 2 ms ; $n_I \sim 1$). However, despite the 9-fold higher amount of hydrous species, the hydrogen-bonded C-OH carbons which are the most efficient sites for CP transfer represent a large part of the HHCP and MC-CP signals (Fig. 10). These findings may be related to previous studies of GO. Panich et al (84) have observed that the static room temperature (RT) ^{1}H NMR spectrum of GO is a narrow line with linewidth $\Delta\upsilon =$ 4.2 kHz attributed to mobile H_2O molecules. The fact that this linewidth is three orders of magnitude greater than the linewidth of liquid water at room temperature implies partial immobilisation, almost certainly because of hydrogen-bonding between the water and GO. Indeed, different types of motion of confined water and functional groups have been previously proposed in GO (85). The simulations of Fig. S7 (ESI) demonstrate that this observation is consistent with our ^{1}H MAS spin-echo NMR spectrum (ESI Fig. S1). Both the static and MAS RT ^{1}H spectra are the sum of two components : (i) a line in fast-exchange narrowing corresponding to H_2O molecules undergoing large amplitude rotational motion with a correlation time τ_C ; (ii) a line in slow-exchange narrowing due to spin diffusion with a bath correlation time τ_B corresponding to rigid hydrogen-bonded C-OH groups. Whereas the line already narrowed by molecular reorientations (and possibly translations) is little affected by MAS the rigid-lattice spectrum is strongly averaged by MAS, resulting in line narrowing in the strong collision limit ($\omega_r\tau_B \gg 1$). The narrow line of the tumbling water molecules representing a large fraction of the signal dominates the RT static ^{1}H spectrum

(ESI Fig. S7(a)) in agreement with the data of Panich et al (84). By contrast, in spin-echo MAS experiments, ^{1}H lineshapes in fast and slow-exchange narrowing may have similar linewidths due to MAS averaging (ESI Fig. S7(b)) and intensities (due to different T_2^H relaxation times), as observed in the non-quantitative spectrum of Fig. S1 ($\tau = 333.33$ μs). Furthermore, components (i) and (ii) lead to with very different $T_{1\rho}^H$ relaxation times in good agreement with our ^{1}H relaxation results (ESI Fig. S4). Indeed, spatial averaging due to random molecular motion with $\tau_C = 0.2 - 0.4$ μs fits well with the fact that $T_2^H = T_{1\rho}^H \sim 0.1$ ms for the signal assigned to fast-relaxing water molecules ($\omega_{1H}\tau_C \ll 1$). On the other hand, since coherent spatial averaging due to MAS at $\nu_r = 18$ kHz and spin fluctuations with $\tau_B = 0.1$ ms have no significant effects on $T_{1\rho}^H$, the hydrogen-bonded C-OH protons under rigid-lattice conditions are likely to relax via spin diffusion towards sinks. A sink is a part of the material where relaxation is very fast. Obviously, the tumbling water molecules ($T_{1\rho}^H \approx 0.1$ ms) may be considered as efficient relaxation sinks in GO. This implies that spin diffusion towards the sinks in a time $T_{1\rho}^H \approx 2$ms is then the rate-controlling step.

Conclusions

The characteristic features of evolutions of magnetization in HHCP and MC-CP experiments were investigated using the simple solutions of the spin thermodynamic equations (classical *I-S* model). Furthermore, using the memory function approach and the Anderson-Weiss (AW) approximation, we have derived analytical solutions to the quantum mechanical (QM) master equation for HHCP and MC-CP dynamics in the case of a multiple-spin system in the presence of random molecular motions (non-classical *I-I*-S* model). The range of validity of both the simplified thermodynamic (*I-S*) and AW (*I-I*-S*) expressions has been evaluated by comparison with exact numerical integration of the QM master equation.

HHCP is found to be inefficient in GO due to fast spin-lattice relaxation of the ^{1}H spins in the rotating frame ($T_{1\rho}^H$). By contrast, the MC-CP technique which alleviates most of the magnetization loss by $T_{1\rho}^H$ relaxation leads to a much larger polarization transfer efficiency

which in turn provides a dramatic reduction in measuring time. Moreover, a detailed analysis of the HHCP and MC-CP kinetics shows the existence of at least two different types of C-OH functional groups although a unique ^{13}C resonance is observed, the major fraction of the hydroxy carbons being in the slow CP regime in which the rate of $T_{1\rho}^{H}$ relaxation is fast compared to the CP rate. This unusual CP regime has been reported for ^{1}H-^{19}F or ^{19}F-^{13}C transfer in polymer systems (86) (87) and ^{1}H-^{29}Si CP in some inorganic compounds (51) (53) (54) (55). However, to the best of our knowledge, the slow CP regime has not been previously observed in organic polyaromatic nanomaterials such as GO. The complementarity of the HHCP and MC-CP experiments in determining the CP regime or its possible mixed character has been clearly demonstrated. The major ^{13}C signal component in the slow CP regime is likely to be mobile functional groups interacting preferentially with fast-relaxing water molecules while the remaining carbons (in the usual fast CP regime) strongly coupled with hydroxyl protons may be assigned to C-OH groups involved in hydrogen bonding (83). Hence, our work also underlines the important role of water in GO (43) (84) (85).

In conclusion, a general strategy to obtain unique structural and motional informations from the kinetics of HHCP and MC-CP has been presented and applied successfully to GO. Notably, in the slow CP regime, the CP time constants cannot be extracted from the kinetics of HHCP alone and their measurement is best accomplished by recording MC-CP build-up curves preferably at several durations of the individual contacts. Since this situation probably arises in functionalized GO (47) (88) and other disordered systems the method presented in this paper is expected to be of great value in elucidating the structures, dynamics, and interactions at interfaces in functional nanomaterials.

Appendix A : Classical *I-S* Model

The general solution of Eqs (1) and (2) (main text) under the initial conditions (at time t_0) $\beta_S(t_0)$ and $\beta_I(t_0)$ can be expressed as (4)

$$\beta_S(t_0+t)=\frac{1}{a_+-a_-}\Big\{[(\varepsilon+\lambda_I-a_-)\beta_S(t_0)+\beta_I(t_0)]\exp\left(-\frac{a_-t}{T_{IS}}\right)$$
$$-[(\varepsilon+\lambda_I-a_+)\beta_S(t_0)+\beta_I(t_0)]\exp\left(-\frac{a_+t}{T_{IS}}\right)\Big\} \quad (A.1)$$

$$\beta_I(t_0+t)=\frac{1}{a_+-a_-}\Big\{[(1+\lambda_S-a_-)\beta_I(t_0)+\varepsilon\beta_S(t_0)]\exp\left(-\frac{a_-t}{T_{IS}}\right)$$
$$-[(1+\lambda_S-a_+)\beta_I(t_0)+\varepsilon\beta_S(t_0)]\exp\left(-\frac{a_+t}{T_{IS}}\right)\Big\}, \quad (A.2)$$

where

$$a_\pm=a_0\pm\sqrt{a_0^2-b} \quad (A.3)$$

with

$$a_0=\frac{1}{2}(1+\varepsilon+\lambda_I+\lambda_S) \quad (A.4)$$

and

$$b=\lambda_I(1+\lambda_S)+\varepsilon\lambda_S. \quad (A.5)$$

The other parameters are the spin-population and relaxation-time ratios :

$$\varepsilon=\frac{N_S}{N_I}\ ;\ \lambda_I=\frac{T_{IS}}{T_{1\rho}^I}\ ;\ \lambda_S=\frac{T_{IS}}{T_{1\rho}^S}. \quad (A.6)$$

Since the initial conditions are $\beta_S(0)=0$ and $\beta_I(0)=\beta_{I0}$ for the the basic HHCP experiment, Eq. (A.1) with $t_0=0$ reduces to the general HHCP double-exponential equation (4) (8) (28)

$$\langle S_z\rangle(t_{CP})=\frac{\beta_S(t_{CP})}{\beta_{I0}}=\frac{1}{a_+-a_-}\left\{\exp\left(-\frac{a_-t_{CP}}{T_{IS}}\right)-\exp\left(-\frac{a_+t_{CP}}{T_{IS}}\right)\right\}. \quad (A.7)$$

When $\varepsilon=0$ and $\lambda_S=0$ Eq. (A.7) yields a particularly simple expression which is given by Eq. (4) (main text). Note also that, in the case of negligible $T_{1\rho}^I$ relaxation ($\lambda_I\ll 1$), we have $a_+-a_-\approx 1+\varepsilon$ so that only half of the initial polarization of the *I* spins can be transferred to the *S* spins if $\varepsilon=1$. Applying Eq. (A.7), it is readily shown that the *S* spin magnetization reaches a maximum value $\langle S_z\rangle_{MAX}^{HH}$ at time t_{MAX}^{HH} defined by (4)

$$\langle S_z \rangle_{MAX}^{HH} = \frac{1}{a_+ - a_-}\left\{\left(\frac{a_-}{a_+}\right)^{\frac{a_-}{a_+ - a_-}} - \left(\frac{a_-}{a_+}\right)^{\frac{a_+}{a_+ - a_-}}\right\}, \quad \text{(A. 8)}$$

and

$$t_{MAX}^{HH} = \frac{T_{IS}}{a_+ - a_-}\ln\left(\frac{a_+}{a_-}\right). \quad \text{(A. 9)}$$

The evolution of β_S given by Eq. (A.1) can be rewritten as

$$\beta_S(t_0 + t) = \frac{\beta_I(t_0)}{a_+ - a_-}\left\{\exp\left(-\frac{a_- t}{T_{IS}}\right) - \exp\left(-\frac{a_+ t}{T_{IS}}\right)\right\} + \beta_S(t_0)X(t), \quad \text{(A. 10)}$$

where

$$X(t) = \frac{1}{a_+ - a_-}\left\{(\varepsilon + \lambda_I - a_-)\exp\left(-\frac{a_- t}{T_{IS}}\right) - (\varepsilon + \lambda_I - a_+)\exp\left(-\frac{a_+ t}{T_{IS}}\right)\right\}. \quad \text{(A. 11)}$$

Assuming full re-equilibration of the *I* spins to the lattice temperature during each mixing step of the MC-CP pulse sequence (Fig. 2), *i.e.*, $T_1^I \ll \tau_M$, we have $\beta_I(\tau_k) = \beta_{I0}$ with $\tau_k = k(t_{CP}/n + \tau_M)$. Furthermore, if $\tau_M \ll T_1^S$ the *S* magnetization is retained during τ_M (β_S remains constant), *i.e.*, $\beta_S(\tau_{k+1}) = \beta_S(\tau_k + t_{CP}/n)$. Hence, the following recursion relation for the evolution of the inverse temperature of the *S* spins during each cycle of the MC-CP sequence is valid :

$$\begin{aligned}\beta_S(\tau_{k+1}) &= \frac{\beta_{I0}}{a_+ - a_-}\left\{\exp\left(-\frac{a_- t_{CP}}{nT_{IS}}\right) - \exp\left(-\frac{a_+ t_{CP}}{nT_{IS}}\right)\right\} + \beta_S(\tau_k)X(t_{CP}/n) \\ &= \beta_S(t_{CP}/n) + \beta_S(\tau_k)X(t_{CP}/n). \quad \text{(A. 12)}\end{aligned}$$

Therefore, $\beta_S(t_{CP} + N\tau_M)$ can be generally expressed as the geometric series

$$\beta_S(t_{CP} + N\tau_M) = \beta_S(t_{CP}/n)[1 + X(t_{CP}/n) + X^2(t_{CP}/n) + \cdots + X^N(t_{CP}/n)]. \quad \text{(A. 13)}$$

The final result is then

$$\langle S_z\rangle(t_{CP}+N\tau_M)=\langle S\rangle_{\infty}^{MC}\big(1-X^n(t_{CP}/n)\big), \qquad (A.14)$$

where

$$\langle S\rangle_{\infty}^{MC}=\frac{\langle S_z\rangle(t_{CP}/n)}{1-X(t_{CP}/n)}. \qquad (A.15)$$

and $\langle S_z\rangle(t_{CP}/n)$ and $X(t_{CP}/n)$ are given by Eqs (A.7) and (A.11). Eq. (A.14) shows that the MC-CP dynamics is exponential with a time constant

$$T_{IS}^{MC}=\frac{-t_{CP}}{n\ln\big(X(t_{CP}/n)\big)}. \qquad (A.16)$$

Although T_{IS}^{MC} approaches T_{IS} when $t_{CP}/n \ll T_{IS}$ the time constant T_{IS}^{MC} is generally longer than T_{IS} unless the number of *S* spins is negligibly small ($\varepsilon \ll 1$) and/or $T_{IS} \gg T_{1\rho}^{I}$ ($T_{IS}^{MC} \approx T_{IS}$). Fortunately, the relative magnitude (heat capacity) and $T_{1\rho}$ relaxation of an extremely diluted spin bath, such as ^{13}C and ^{15}N, can often be neglected ($\varepsilon = 0$ and $\lambda_S = 0$) so that Eqs (A.3) - (A.6) yield $a_{\pm}=1$ and $a_{\mp}=\lambda_I$ (case $\lambda_I < 1$ or $\lambda_I > 1$) and Eqs (A.7) and (A.14) reduce to Eqs (4) and (5) (main text).

Appendix B : Non-classical *I-I*-S* Model

Following the usual treatment of second-order perturbation theory, the spin dynamics of the reduced density operator in the simplest case of a *I*-S* spin pair ($n_I = 1$) including rotating-frame spin-lattice ($T_{1\rho}$) relaxation is given by the generalized Liouville-von Neumann differential equation (29) (30)

$$\frac{d}{dt}\hat{\sigma}(t)=-i\big[\hat{H}(t),\hat{\sigma}(t)\big]-\hat{\hat{\Gamma}}\left\{\hat{\sigma}(t)-\hat{\sigma}_{\infty}e^{-t/T_{1\rho}^{I}}\right\}-\hat{\hat{\mathrm{R}}}\{\hat{\sigma}(t)\} \qquad (B.1)$$

with the Hamiltonian

$$\hat{H}(t) = \omega_{1I}\hat{I}_z + \omega_{1S}\hat{S}_z + 2b(t)\hat{I}_x\hat{S}_x, \qquad \text{(B. 2)}$$

where ω_{1I} and ω_{1S} are the amplitudes of the radiofrequency (RF) fields applied to the *I* and *S* spins and $b(t)$ is given by Eq. (8) (main text). The initial and final density operators, $\hat{\sigma}(0)$ and $\hat{\sigma}_\infty$, are $\hat{I}_z$ and $\hat{I}_z + \hat{S}_z$, respectively. For a fast fluctuating *I*-spin bath, the spin diffusion superoperator $\hat{\hat{\Gamma}}$ can be written as

$$\hat{\hat{\Gamma}}(\sigma) = R_{dp}\left[\hat{I}_z, \left[\hat{I}_z, \sigma\right]\right] + R_{df}\left\{\left[\hat{I}_x, \left[\hat{I}_x, \sigma\right]\right] + \left[\hat{I}_y, \left[\hat{I}_y, \sigma\right]\right]\right\}. \qquad \text{(B. 3)}$$

$\hat{\hat{\Gamma}}$ then depends on two rate constants, $R_{dp} = 1/T_{dp}$ and $R_{df} = 1/T_{df}$. As R_{df} is associated with the flip-flop term of the homonuclear (*I-I**) dipolar Hamiltonian (XY or planar term) (69) its role in transferring polarization can be easily interpreted. Hence, R_{df} allows the complete thermal equilibration with the bath. The effect of R_{dp} is more subtle : it can be associated with a process where the environment *observes* the system breaking its coherences (Ising term) (89) driving the system to the internal quasiequilibrium (90). Actually, T_{dp} and T_{df} may be respectively regarded as the spin-spin (T_2) and spin-lattice (T_1) relaxation times of the *I** spin in a random fields mode. Indeed, for a dipolar interaction Hamiltonian in strong RF fields ($\omega_{1I} \gg \omega_r$), R_{dp} and R_{df} can be expressed as (25) (91)

$$R_{dp} = \frac{N_2^{II}}{3}\left[\frac{2\tau_x}{1 + (\omega_r\tau_x)^2} + \frac{\tau_x}{1 + 4(\omega_r\tau_x)^2}\right] \qquad \text{(B. 4)}$$

and

$$R_{df} \approx \frac{N_2^{II}}{4}\frac{\tau_x}{1 + (\omega_{1I}\tau_x)^2}, \qquad \text{(B. 5)}$$

where N_2^{II} is the second moment of the dipolar fluctuation autocorrelation function and τ_x is the correlation time of the *I*-spin bath in the rotating frame. Note that Eqs (B.4) and (B.5) give $R_{dp}/R_{df} = 4$ in the extreme narrowing regime ($\omega_{1I}\tau_x \ll 1$) (69). The phenomenological relaxation superoperator $\hat{\hat{\mathrm{R}}}$ for the *I*-S* system is assumed to satisfy the relaxation rate equations

$$\frac{d}{dt}\left(\sigma_{11}^{rel}(t) - \sigma_{44}^{rel}(t)\right) = -\frac{R_{1\rho}^{\Sigma}}{2}\left(\sigma_{11}(t) - \sigma_{44}(t)\right) - \frac{R_{1\rho}^{\Delta}}{2}\left(\sigma_{33}(t) - \sigma_{22}(t)\right) \qquad \text{(B. 6)}$$

$$\frac{d}{dt}\left(\sigma_{33}^{rel}(t) - \sigma_{22}^{rel}(t)\right) = -\frac{R_{1\rho}^{\Delta}}{2}\left(\sigma_{11}(t) - \sigma_{44}(t)\right) - \frac{R_{1\rho}^{\Sigma}}{2}\left(\sigma_{33}(t) - \sigma_{22}(t)\right), \qquad \text{(B. 7)}$$

where

$$R_{1\rho}^{\Sigma} = \frac{1}{T_{1\rho}^{I}} + \frac{1}{T_{1\rho}^{S}} \qquad \text{and} \qquad R_{1\rho}^{\Delta} = \frac{1}{T_{1\rho}^{I}} - \frac{1}{T_{1\rho}^{S}}. \qquad \text{(B. 8)}$$

The time dependence of $b(t)$ makes the derivation of general (*non-secular*) solutions to the quantum mechanical (QM) equation (Eq. (B.1)) a formidable task (25) (70). A simple analytical solution for the polarization of the *S* spin, $\langle S_z\rangle(t) = Tr\left(\hat{\sigma}(t)\hat{S}_z\right)$, is obtained only when the HH matching condition is exactly fulfilled in the *secular* approximation, *i.e.*, under the conditions $\omega_{1I} = \omega_{1S} \gg D_{IS} \gg R_{dp}, R_{df} \gg 1/T_{1\rho}^{I}, 1/T_{1\rho}^{S}$ (25) (29) (30) (69) (70).

We have recently derived non-secular analytical solutions to the QM master equation for HHCP and MC-CP dynamics that are valid for arbitrary values of the applied RF fields and spinning frequency by using a combination of the memory function approach and the Anderson-Weiss (AW) approximation (25). This simple formalism is extended below to the case of a multiple-spin system $I_{n_I}^{*}$- *S* ($n_I > 1$) in the presence of lattice motion. In strong RF fields ($\Sigma = \omega_{1I} + \omega_{1S} \gg D_{IS}$) and neglecting $T_{1\rho}$ relaxation, the polarizations of a particular *S* spin (^{13}C), $\langle S_z\rangle(t)$, and its n_I neighboring *I** spins (^{1}H), $n_I\langle I_z\rangle(t)$, may be described by the differential equations (58) (68)

$$\frac{d}{dt}\langle S_z\rangle(t) = -n_I \frac{d}{dt}\langle I_z\rangle(t) = -\int_0^t K_\Delta(t-t')[\langle S_z\rangle(t') - \langle I_z\rangle(t')]dt'. \qquad \text{(B. 9)}$$

Eqs (B.9) describe a non-Markovian process because they contain the memory function $K_\Delta(\tau)$. An ansatz form for $K_\Delta(\tau)$ in a powder CPMAS experiment is given by (25) (65) (71) (92) (93)

$$K_\Delta(\tau) = \frac{M_2^{IS}}{2} K_{MAS}(\tau) g(\tau) \cos(\Delta\tau) \exp\left(-R_{dp}\tau\right), \qquad \text{(B. 10)}$$

where M_2^{IS} is the powder-averaged heteronuclear second moment (72) of the $I_{n_I}^*$- *S* spin system ($M_2^{IS} = D_{IS}^2/5$ if $n_I = 1$) and $\Delta = \omega_{1I} - \omega_{1S}$. MAS introduces a modulation of the interactions at the angular frequency ω_r :

$$K_{MAS}(\tau) = \frac{2}{3}\cos(\omega_r\tau) + \frac{1}{3}\cos(2\omega_r\tau). \qquad \text{(B. 11)}$$

Molecular reorientations give rise to local fluctuations in the $I_{n_I}^*$- *S* dipolar field. It is not difficult to include such motional effects in $K_\Delta(\tau)$. Their associated correlation function

$$g(\tau) = (1-S^2)\exp\left(-\frac{\tau}{\tau_c}\right) + S^2 \qquad \text{(B. 12)}$$

is defined by an order parameter S and a correlation time τ_c.

In the fast-correlation limit ($\sqrt{M_2^{IS}}T_{dp} \ll 1$), note that the following CP rate is obtained :

$$\frac{1}{T_{IS}} = \int_0^\infty K_\Delta(\tau)d\tau = \frac{M_2^{IS}}{4} j(\omega_{1I} - \omega_{1S}), \qquad \text{(B. 13)}$$

where

$$j(\omega) = (1-S^2)K(\omega, 1/\tau_c) + S^2 K(\omega, 0) \qquad \text{(B. 14)}$$

with

$$K(\omega, 1/\tau_c) = \frac{1}{3}\left[L\left(\omega - \omega_r, 1/\tau_c + R_{dp}\right) + L\left(\omega + \omega_r, 1/\tau_c + R_{dp}\right)\right]$$

$$+\frac{1}{6}\left[L\left(\omega - 2\omega_r, 1/\tau_c + R_{dp}\right) + L\left(\omega + 2\omega_r, 1/\tau_c + R_{dp}\right)\right] \qquad \text{(B. 15)}$$

and

$$L(\Omega, \Gamma) = \frac{2\Gamma}{\Gamma^2 + \Omega^2}. \qquad \text{(B. 16)}$$

$j(\omega)$ is the reduced spectral density defined in Refs (92) (93). Furthermore, Eqs (B.9) become identical to Eqs (1) and (2) (*I-S* model) replacing $\langle S_z \rangle$, $\langle I_z \rangle$ and $1/n_I$ by β_S, β_I and ε, respectively, and adding $T_{1\rho}^I$ and $T_{1\rho}^S$ spin-lattice relaxation terms. Hence, as expected, the *I-I*-S* model is completely equivalent to the theoretical analysis of CPMAS dynamics developed by Topgaard and coworkers (92) (93) when $\sqrt{M_2^{IS}} T_{dp} \ll 1$ (fast-correlation limit) and $n_I \gg 1$ (*I-S* model with $\varepsilon \approx 0$). Note that the spin dynamics obtained with the non-classical *I-I*-S* model ($n_I = 1$) through Eq. (B.1) also converges with the classical *I-S* calculation when $\sqrt{M_2^{IS}} T_{df} \ll 1$ with $1/T_{IS} = M_2^{IS} T_{df}/2$ and $\epsilon = 0$.

Although the simplifying fast-correlation assumption is practical for predicting CP signal intensities under MAS (65) (92) (93) a more rigorous approach based on the popular AW model (73) (74) (75) accounting for the non-Markovian character of the spin dynamics must be used when analyzing HHCP and MC-CP build-up curves at short contact times (25) (58). Such a more accurate description is presented in the following. It is first remarked that Eqs (B.9) can be rewritten as

$$\frac{d}{dt}\langle I_z - S_z \rangle(t) = -\frac{n_I + 1}{n_I} \int_0^t K_\Delta(t - t') \langle I_z - S_z \rangle(t') dt' \qquad \text{(B. 17)}$$

$$\frac{d}{dt}\langle n_I I_z + S_z\rangle(t) = 0. \qquad \text{(B. 18)}$$

Eq. (B.18) agrees with the fact that the total polarization of the S-$I^*_{n_I}$ spin system ($\langle n_I I_z + S_z\rangle$) is still a constant of the motion and therefore conserved under MAS when the amplitudes of the applied RF fields are much larger than the spinning rate and the $I^*_{n_I}$- S dipolar couplings ($\omega_{1I}, \omega_{1S} \gg \omega_r, \sqrt{M_2^{IS}}$) (94). The AW approximation (74) (75) may then be used to derive a simple analytical solution to Eq. (B.17) for $\langle I_z - S_z\rangle$:

$$\frac{d}{dt}\langle I_z - S_z\rangle(t) = -\frac{n_I + 1}{n_I}\int_0^t K_\Delta(\tau)\langle I_z - S_z\rangle(t-\tau)d\tau$$

$$\approx -\frac{n_I + 1}{n_I}\langle I_z - S_z\rangle(t)\int_0^t K_\Delta(\tau)d\tau. \qquad \text{(B. 19)}$$

Substituting Eq. (B.10) into Eq. (B.19), one finds the solution

$$\langle I_z - S_z\rangle(t_0 + t) = \langle I_z - S_z\rangle(t_0)G(t), \qquad \text{(B. 20)}$$

where t_0 is the initial time and

$$G(t) = \exp\left[-\frac{n_I + 1}{2n_I}\int_0^t (t-\tau)\, K_\Delta(\tau)d\tau\right]$$

$$= \exp\left\{\frac{n_I + 1}{2n_I}\left[M_2^{IS}S^2F\left(R_{dp}, \Delta, \omega_r, t\right) + M_2^{IS}(1-S^2)F\left(1/\tau_c + R_{dp}, \Delta, \omega_r, t\right)\right]\right\} \qquad \text{(B. 21)}$$

with

$$F(x, \Delta, \omega_r, t) = \frac{1}{3}[f(x, \Delta - \omega_r, t) + f(x, \Delta + \omega_r, t)]$$

$$+\frac{1}{6}[f(x,\Delta-2\omega_r,t)+f(x,\Delta+2\omega_r,t)]. \qquad \text{(B. 22)}$$

The $f(x,\omega,t)$ function is defined in Refs (74) (75).

Eqs (B.18) and (B.20) give simple expressions of the HHCP and MC-CP build-up curves under MAS for an $I_{n_I}^*$- S spin system interacting with a fast fluctuating I-spin bath in the presence of molecular dynamics in the intermediate regime neglecting contact with the lattice through $T_{1\rho}^I$ and $T_{1\rho}^S$ relaxation. However, since the relevant parameters for $j(\omega)$ then are ω_{1I} and ω_{1S} ($\omega_r \ll \omega_{1I},\omega_{1S}$) efficient $T_{1\rho}$ relaxation is expected in the presence of motions with medium-to-slow correlation times (milliseconds to nanoseconds). Considering only homonuclear dipolar relaxation for the *I* spins and heteronuclear dipolar relaxation for the *S* spins ($\varepsilon = N_S/N_I \ll 1$) and neglecting spectral density terms around ω_{0I} and ω_{0S}, the relaxation rates for one reorientational process of correlation time τ_c in a powder sample are written (95) (96)

$$\frac{1}{T_{1\rho}^I}=\frac{1}{2}M_2^{II}j(2\omega_{1I}) \qquad \text{(B. 23)}$$

$$\frac{1}{T_{1\rho}^S}=\frac{1}{2}M_2^{IS}j(\omega_{1S}), \qquad \text{(B. 24)}$$

where M_2^{II} is the powder-averaged homonuclear second moment (72) and $j(\omega)$ is given by Eq. (B.14). $T_{1\rho}^I$ and $T_{1\rho}^S$ relaxation is readily taken into account in the fast-correlation limit ($\sqrt{M_2^{IS}}T_{dp} \ll 1$) since the HHCP and MC-CP dynamics are then obtained by solving Eq. (1) and (2) (classical *I*-*S* model) with $\varepsilon \equiv \varepsilon^* = N_S/N_I^* = 1/n_I$ and T_{IS} given by Eq. (B.13). Such a straightforward analysis cannot be made when memory effects of the *I* spin bath are important, *i.e.*, $\sqrt{M_2^{IS}}T_{dp} \gtrsim 1$ (the usual case for the *I*-*I**-*S* model) (25) (58). However, as long as spin-lattice relaxation in the rotating frame is relatively slow ($\sqrt{M_2^{IS}}T_{1\rho}^I, \sqrt{M_2^{IS}}T_{1\rho}^S \gg 1$), the following expression for the evolution of the *S* polarization during CP is readily obtained by using the first-order approximation of the *I*-*S* model solution ($\lambda_I, \lambda_S \ll 1$) :

$$\langle S_z\rangle(t_0+t_{CP})=\frac{1}{n_I+1}[\langle n_I I_z+S_z\rangle(t_0)e^{-R_1 t_{CP}}-n_I\langle I_z-S_z\rangle(t_0)e^{-R_2 t_{CP}}G(t_{CP})], \tag{B.25}$$

where

$$R_1=\frac{1}{n_I+1}\left(\frac{n_I}{T_{1\rho}^I}+\frac{1}{T_{1\rho}^S}\right) \tag{B.26}$$

$$R_2=\frac{1}{n_I+1}\left(\frac{1}{T_{1\rho}^I}+\frac{n_I}{T_{1\rho}^S}\right). \tag{B.27}$$

It must be pointed out that Eq. (B.25) holds whatever the spin-lattice relaxation rate if $T_{1\rho}^I=T_{1\rho}^S$, *i.e.*, $R_{1\rho}^{\Delta}=0$ ($R_1=R_2$). Note also that $R_1=R_2$ if $n_I=1$.

Using the initial conditions at $t_0=0$ for HHCP, $\langle I_z\rangle(0)=1$, $\langle S_z\rangle(0)=0$, the *S* spin polarization as a function of the contact time t_{CP} is easily calculated to be

$$\langle S_z\rangle(t_{CP})=\frac{n_I}{n_I+1}[e^{-R_1 t_{CP}}-e^{-R_2 t_{CP}}G(t_{CP})]. \tag{B.28}$$

Note that the equilibrium state polarization reached in the absence of spin-lattice relaxation ($R_1=R_2=0$), $\langle S_z\rangle(\infty)=n_I/(n_I+1)$, which agrees with the one calculated in the thermodynamic limit (the mean magnetization at each site) (94) is significantly higher than the time averaged value in an isolated SI_{n_I} spin system ($R_{dp}=0$) (34) (97). $\langle S_z\rangle(\infty)$ is then in principle overestimated (and n_I is underestimated) when $\sqrt{M_2^{IS}}T_{dp}\gg 1$. It is however well known that $\langle S_z\rangle(\infty)$ is actually a quasi-equilibrium state polarization since the XY term of the homonuclear (*I-I**) dipolar Hamiltonian has been neglected in our analysis of the *I-I*-S* model ($R_{df}=0$). Indeed, in the absence of spin lattice relaxation ($T_{1\rho}$), the XY term is responsible for the exponential approach of $\langle S_z\rangle(t_{CP})$ towards the final equilibrium state with a rate R_{df} (69) (70). We and others (58) (69) (98) have observed that R_{dp} is often much higher than R_{df}, *i.e.*, the *I-I** interaction reveals a highly anisotropic behavior ($R_{dp}/R_{df}\gg$

1). This may be related to the fact that R_{dp} and R_{df} are expected to be given by Eqs (B.4) and (B.5), respectively. Since $R_{dp} \gg R_{df}$ when $\omega_{1I} \gg \omega_r$ and $\omega_{1I}\tau_x > 1$, a slow-fluctuation regime of the local fields, controlled by the spin dynamics of the bath, could explain these experimental observations (69). Moreover, in a « real » system of N_I spins where there is a strongly coupled $SI_{n_I}^*$ cluster and $N_I - n_I$ remote (weakly coupled) *I* spins the quasi-equilibrium polarization at long times $\langle S_z \rangle_{qe}$ will be proportional to $N_I/(N_I + 1)$ (26) (33). In other words, the amplitude of the second stage of the HHCP dynamics is reduced by the finite energy of the *I*-spin bath. In any case, the transfer of spin order by SD may be neglected when the *I* and/or *S* magnetizations decay rapidly due to spin-lattice relaxation in the rotating frame $T_{1\rho}^I$ and/or $T_{1\rho}^S < T_{df}$).

In MC-CP, assuming full repolarization of the *I** spin(s) during each mixing time ($T_1^I \ll \tau_M$), we have $\langle I_z \rangle(\tau_k) = 1$. Moreover, assuming that $\tau_M \ll T_1^S$, the *S* polarization is unchanged during each mixing step. Hence, the following recursion relation for MC-CP is deduced from Eq. (B.25) :

$$\langle S_z \rangle(\tau_{k+1}) = \frac{1}{n_I + 1}\left\{[n_I + \langle S_z \rangle(\tau_k)]e^{-R_1 t_{CP}/n} - n_I[1 - \langle S_z \rangle(\tau_k)]e^{-R_2 t_{CP}/n} G(t_{CP}/n)\right\}$$

$$= \frac{1}{n_I + 1}\Big[n_I\left(e^{-R_1 t_{CP}/n} - e^{-R_2 t_{CP}/n} G(t_{CP}/n)\right) + \langle S_z \rangle(\tau_k)\left(e^{-R_1 t_{CP}/n} + n_I e^{-R_2 t_{CP}/n} G(t_{CP}/n)\right)\Big]$$

$$= \langle S_z \rangle(t_{CP}/n) + \langle S_z \rangle(\tau_k) X(t_{CP}/n), \qquad \text{(B. 29)}$$

where $\tau_k = k(t_{CP}/n + \tau_M)$ and

$$X(t) = \frac{e^{-R_1 t}}{n_I + 1} + \frac{n_I e^{-R_2 t}}{n_I + 1} G(t). \qquad \text{(B. 30)}$$

The MC-CP dynamics is readily obtained from Eq. (B.29) :

$$\langle S_z\rangle(t_{CP}+N\tau_M)=\frac{\langle S_z\rangle(t_{CP}/n)}{1-X(t_{CP}/n)}[1-X^n(t_{CP}/n)]. \qquad (\mathrm{B}.31)$$

As expected, Eq. (B.31) reduces to Eq. (45) of Ref. (25) ($R_{df}=0$) when $R_1=R_2=0$ and $n_I=1$.

Acknowledgements

The authors are grateful to the French Ministry of Research, the Centre National de la Recherche Scientifique (CNRS), the University of Strasbourg and the international center for Frontier Research in Chemistry (icFRC) for their help in establishing and maintaining the solid-state NMR platform. We gratefully acknowledge the financial support from the Agence Nationale de la Recherche (ANR) through the LabEx project Chemistry of Complex Systems (ANR-10-LABX-0026_CSC). The authors also wish to thank Nadia Achour for her help at the early stage of this project.

Notes and references

1 A. Pines, M. G. Gibby, J. S. Waugh, *J. Chem. Phys.,* 1972, **56**, 1776-1777.
2 A. Pines, M. G. Gibby, J. S. Waugh, *J. Chem. Phys.*, 1973, **59**, 569-590.
3 J. Schaefer, E. O. Stejskal, *J. Am. Chem. Soc.,* 1976, **98**, 1031-1032.
4 M. Mehring, *Principles of High Resolution NMR in Solids.* Berlin : Springer-Verlag, 1983.
5 C. A. Fyfe, *Solid State NMR for Chemists.* Guelf : C. F. C. Press, 1983.
6 V. J. McBrierty, K. J. Packer, *Nuclear magnetic resonance in solid polymers.* Cambridge : Cambridge University Press, 1993.
7 E. O. Stejskal, J. D. Memory, *High-Resolution NMR in the Solid State: Fundamentals of CP/MAS.* New York : Oxford University Press, 1994.
8 W. Kolodziejski, J. Klinowski*, Chem. Rev.*, 2002, **102**, 613-628.
9 L. B. Alemany, D. M. Grant, R. J. Pugmire, T. D. Alger, K. W. Zilm., *J. Am. Chem. Soc.*, 1983, **105**, 2133-2141.
10 N. Zumbulyadis, J. M. O'Reilly, *J. Magn. Reson.*, 1989, **82**, 613-618.
11 G. Metz, M. Ziliox, S. O. Smith, *Solid State Nucl. Magn. Reson.*, 1996, **7**, 155-160.
12 R. Fu, J. Hu, T. A. Cross, J. Magn. Reson., 2004, **168**, 8-17.
13 G. Hou, F. Deng, S. Ding, R. Fu, J. Yang, C. Ye, *Chem. Phys. lett.*, 2006, **421**, 356-360.
14 G. Hou, F. Deng, C. Ye, S. Ding, *J. Chem. Phys.*, 2006, **124**, 234512.

15 K. Takeda, Y. Noda, K. Takegoshi, O. Lafon, J. Trébosc, J. P. Amoureux, *J. Magn. Reson.*, 2012, **214**, 340-345.
16 S. Zhang, X. Wu, M. Mehring, *Chem. Phys. Lett.*, 1990, **166**, 92-94.
17 G. Jeschke, G. Grossmann, *J. Magn. Reson. Ser. A*, 1993, **103**, 323-328.
18 M. Melchior, *24th Rocky Mountain Conference,* 1982.
19 B. C. Gerstein, C. Dybowsky**,** *Transient Techniques in NMR of solids: an Introduction to Theory and Practice.* San Diego : Academic Press*,* 1985.
20 R. L. Johnson, K. Schmidt-Rohr*, J. Magn. Reson.,* 2014*,* **239***,* 44-49.
21 P. Duan, K. Schmidt-Rohr*, J. Magn. Reson.,* 2017, **285**, 68-78.
22 W. Tang, A. A. Nevzorov, *J. Magn. Reson.,* 2011, **212**, 245-248.
23 S. N. Koroloff, A. A. Nevzorov*, J. Magn. Reson.,* 2015, **256**, 14-22.
24 J. Raya, B. Perrone, J. Hirschinger*, J. Magn. Reson.,* 2013, **227**, 93-102.
25 J. Raya, J. Hirschinger*, J. Magn. Reson.,* 2017*,* **281**, 253-271.
26 V. Klimavicius, L. Dagys, V. Chizhik, V. Balevicius, *Appl. Magn. Reson.,* 2017, **48**, 673-685.
27 D. A. McArthur, E. L. Hahn, R. E. Walstedt*, Phys. Rev.,* 1969*,* **188**, 609-638*.*
28 S. Ando, R. K. Harris, S. Reinsberg*, J. Magn. Reson.,* 1999*,* **141**, 91-103.
29 L. Muller, A. Kumar, T. Baumann, R. R. Ernst*, Phys. Rev. Lett.,* 1974, **32**, 1402-1406.
30 A. Naito, C. A. McDowell*, J. Chem. Phys.,* 1986, **84**, 4181-4186*.*
31 K. Takegoshi, C. A. McDowell, *J. Chem. Phys.*, 1987, **86**, 6077-6084.
32 P. Bertani, J. Raya, P. Reinheimer, R. Gougeon, L. Delmotte, J. Hirschinger, *Solid State Nucl. Magn. Reson.*, 1999, **13**, 219-229.
33 C. A. Fyfe, A. R. Lewis, J. M. Chézeau, *Can. J. Chem.*, 1999, **77**, 1984-1993.
34 M. Hologne, P. Bertani, T. Azaïs, C. Bonhomme, J. Hirschinger, *Solid State Nucl. Magn. Reson.*, 2005, **28**, 50-56.
35 P. Paluch, T. Pawlak, J. P. Amoureux, M. J. Potrzebowski, *J. Magn. Reson.*, 2013, **233**, 56-63.
36 P. Paluch, J. Trébosc, Y. Nishiyama, M. J. Potrzebowski, M. Malon, J. P. Amoureux, *J. Magn. Reson.*, 2015, **252**, 67-77.
37 R. Zhang, J. Damron, T. Vosegaard, A. Ramamoorthy, *J. Magn. Reson.*, 2015, **250**, 37-44.
38 R. Gupta, G. Hou, T. Polenova, A. J. Vega, *Solid State Nucl. Magn. Reson.*, 2015, **72**, 17-26.
39 M. Ernst, B. H. Meier, M. Tomaselli, A. Pines, *Mol. Phys.*, 1998, **95**, 849-858.
40 M. Ernst, B. H. Meier, M. Tomaselli, A. Pines, *J. Chem. Phys.*, 1998, **108**, 9611-9613.
41 A. C. Ferrari, F. Bonaccorso, V. Fal'ko, K. S. Novoselov, S. Roche, P. Boggild, S. Borini, F. H. L. Koppens, V. Palermo, N. Pugno, J. A. Garrido, R. Sordan, A. Bianco, L. Ballerini, M. Prato, E. Lidorikis, J. Kivioja, C. Marinelli, T. Ryhänen, A. Morpurgo, J. N. Coleman, V. Nicolosi, L. Colombo, A. Fert, M. Garcia-Hernandez, A. Bachtold, G. F. Schneider, F. Guinea, C. Dekker, M. Barbone, Z. Sun, C. Galiotis, A. N. Grigorenko, G. Konstantatos, A. Kis, M. Katsnelson, L. Vandersypen, A. Loiseau, V. Morandi, D. Neumaier, E. Treossi, V. Pellegrini, M. Polini, A. Tredicucci, G. M. Williams, B. H. Hong, J.-H. Ahn, J. M. Kim, H. Zirath, B. J. van Wees, H. van der Zant, L. Occhipinti, A. Di Matteo, I. A. Kinloch, T. Seyller, E. Quesnel, X. Feng, K. Teo, N. Rupesinghe, P. Hakonen, S. R. T. Neil, Q. Tannock, T. Löfwander, J. Kinaret, *Nanoscale*, 2015, **7**, 4598-4810.
42 G. Reina, J. M. Gonzalez-Dominguez, A. Criado, E. Vazquez, A. Bianco, M. Prato, *Chem. Soc. Rev.,* 2017*,* **46**, 4400-4416.

43 A. Lerf, H. He, M. Foster, J. Klinowski, *J. Phys. Chem. B*, 1998, **102**, 4477-4482.
44 T. Szabo, O. Berkesi, P. Forgo, K. Josepovits, Y. Sanakis, D. Petridis, I. Dekany, *Chem. Mater.*, 2006, **18**, 2740-2749.
45 W. Gao, L. B. Alemany, L. Ci, P. M. Ajayan, *Nat. Chem.*, 2009, **1**, 403-408.
46 A. M. Dimiev, L. B. Alemany, J. M. Tour, *ACS Nano*, 2013, **7**, 576-588.
47 I. A. Vacchi, C. Spinato, J. Raya, A. Bianco, C. Ménard-Moyon, *Nanoscale*, 2016, **8**, 13714-13721.
48 W. Cai, R. D. Piner, F. J. Stadermann, S. Park, M. A. Shaibat, Y. Ishii, D. Yang, A. Velamakanni, S. J. An, M. Stoller, J. An, D. Chen, R. S. Ruoff, *Science*, 2008, **321**, 1815-1817.
49 L. B. Casablanca, M. A. Shaibat, W. W. Cai, S. Park, R. Piner, R. S. Ruoff, Y. Ishii, *J. Am. Chem. Soc.*, 2010, **132**, 5672-5676.
50 M. Goldman, *Spin Temperature and Nuclear Magnetic Resonance in Solids*, Oxford : Clarendon Press, 1970.
51 I. Klur, J. F. Jacquinot, F. Brunet, T. Charpentier, J. Virlet, C. Schneider, P. Tekely, *J. Phys. Chem. B*, 2000, **104**, 10162-10167.
52 P. Tekely, V. Gérardy, P. Palmas, D. Canet, A. Retournard, *Solid State Nucl. Magn. Reson.*, 1995, **4**, 361-367.
53 C. Gardiennet, P. Tekely, *J. Phys. Chem. B*, 2002, **106**, 8928-8936.
54 C. Gardiennet, F. Marica, C. A. Fyfe, P. Tekely, *J. Chem. Phys.,* 2005*,* **122**, 054705.
55 C. A. Fyfe, D. H. Brouwer, P. Tekely, *J. Phys. Chem. A*, 2005, **109**, 6187-6192.
56 X. Wu, S. Zhang, X. Wu, *Phys. Rev. B*, 1988, **37**, 9827-9829.
57 J. Hirschinger, M. Hervé, *Solid State Nucl. Magn. Reson.*, 1994, **3**, 121-135.
58 P. Reinheimer, J. Hirschinger, P. Gilard, N. Goetz, *Magn. Reson. Chem*., 1997, **35**, 757-764.
59 The CP rate may nevertheless depend on the MAS frequency (cf. Eqs (B.13)-(B.16) in Appendix B).
60 R. Zwanzig, *J. Chem. Phys.*, 1960, **33**, 1338-1341.
61 R. Zwanzig, *Physica*, 1964, **30**, 1109-1123.
62 F. Marica, R. F. Snider, *Solid State Nucl. Magn. Reson.*, 2003, **23**, 28-49.
63 X. Wu, K. W. Zilm, *J. Magn. Reson. Ser. A*, 1993, **104**, 154-165.
64 D. E. Demco, J. Tegenfeldt, J. S. Waugh, *Phys. Rev. B*, 1975, **11**, 4133-4151.
65 F. Engelke, T. Kind, D. Michel, M. Pruski, B. Gerstein, *J. Magn. Reson*., 1991, **95**, 286-298.
66 S. Ding, C. McDowell, C. Ye, *J. Magn. Reson. Ser. A*, 1994, **109**, 6-13.
67 H. Mori, *Prog. Theor. Phys*., 1965, **33**, 423-455.
68 T. T. P. Cheung, R. Yaris, *J. Chem. Phys.*, 1980, **72**, 3604-3616.
69 A. K. Chattah, G. A. Alvarez, P. Levstein, F. M. Cucchietti, H. M. Pastawski, J. Raya, J. Hirschinger, *J. Chem. Phys*., 2003, **119**, 7943-7951.
70 J. Hirschinger, J. Raya, *Mol. Phys.*, 2015, **113**, 3161-3175.
71 M. F. Cobo, K. Malinakova, D. Reichert, K. Saalwächter, E. R. deAzevedo, *Phys. Chem. Chem. Phys.*, 2009, **11**, 7036-7047.
72 A. Abragam, *The Principles of Nuclear Magnetism*, Oxford : Oxford University Press, 1961.
73 P. W. Anderson, P. R. Weiss, *Rev. Mod. Phys*., 1953, **25**, 269-276.
74 J. Hirschinger, *Concepts Magn. Reson. Part A*, 2006, **28**, 307-320.
75 J. Hirschinger, *Solid State Nucl. Magn. Reson.*, 2008, **34**, 210-223.

76 B. M. Fung, A. K. Khitrin, K. Ermolaev, *J. Magn. Reson.*, 2000, **142**, 97-101.
77 M. Rance, R. A. Byrd, *J. Magn. Reson.*, 1983, **52**, 221-240.
78 E. T. Olejniczak, S. Vega, R. G. Griffin, *J. Chem. Phys.*, 1984, **81**, 4804-4817.
79 N. J. Brownbill, R. S. Sprick, B. Bonillo, S. Pawsey, F. Aussenac, A. J. Fielding, A. I. Cooper, F. Blanc, *Macromolecules*, 2018, **51**, 3088-3096.
80 V. J. McBrierty, D. C. Douglass, *Phys. Rep.*, 1980, **63**, 61-147.
81 K. Schmidt-Rohr, H. W. Spiess, *Multidimensional Solid-State NMR and Polymers*, London : Academic Press, 1994.
82 J. Raya, J. Hirschinger, S. Ovarlez, F. Giulieri, A. M. Chaze, F. Delamare, *Phys. Chem. Chem. Phys.*, 2010, **12**, 14508-14514.
83 N. Lu, Y. Huang, Z. Li, J. Yang, *J. Chem. Phys.*, 2010, **133**, 034502.
84 A. M. Panich, A. I. Shames, N. A. Sergeev, *Appl. Magn. Reson.*, 2013, **44**, 107-116.
85 A. Buchsteiner, A. Lerf, J. Pieper, *J. Phys. Chem. B*, 2006, **110**, 22328-22338.
86 W. S. Veeman, W. E. J. R. Maas, *Solid State NMR Techniques for the Study of Polymer-Polymer Miscibility*, in *NMR Basic Principles and Progress*, Vol. 32, Berlin : Springer-Verlag, 1994.
87 S. Ando, R. K. Harris, G. A. Monti, S. A. Reinsberg, *Magn. Reson. Chem*., 1999, **37**, 709-720.
88 I. A. Vacchi, J. Raya, A. Bianco, C. Ménard-Moyon, *2D Mater.*, 2018, **5**, 035037.
89 G. A. Alvarez, E. P. Danieli, P. R. Levstein, H. M. Pastawski, *J. Chem. Phys.*, 2006, **124**, 194507.
90 M. H. Levitt, D. Suter, R. R. Ernst, *J. Chem. Phys.*, 1986, **84**, 4243-4255.
91 M. Mehring, V. A. Weberuss, *Object-Oriented Magnetic Resonance*, San Diego : Academic Press, 2001.
92 A. Nowacka, P. C. Mohr, J. Norrman, R. W. Martin, D. Topgaard, *Langmuir*, 2010, **26**, 16848-16856.
93 A. Nowacka, N. A. Bongartz, O. H. S. Ollila, T. Nylander, D. Topgaard, *J. Magn. Reson*., 2013, **230**, 165-175.
94 Meier, B. H., *Chem. Phys. Lett*., 1992, **188**, 201-206.
95 G. P. Jones, *Phys. Rev*., 1966, **148**, 332-335.
96 H. T. Stokes, D. C. Ailion, *Phys. Rev. B*, 1978, **18**, 141-156.
97 G. C. Chingas, A. N. Garroway, R. D. Bertrand, W. B. Moniz, *J. Chem. Phys*., 1981, **74**, 127-156.
98 P. Palmas, P. Tekely, D. Canet, *J. Magn. Reson. Ser. A*, 1993, **104**, 26-36**.**

Figures

Fig. 1

Raya et al

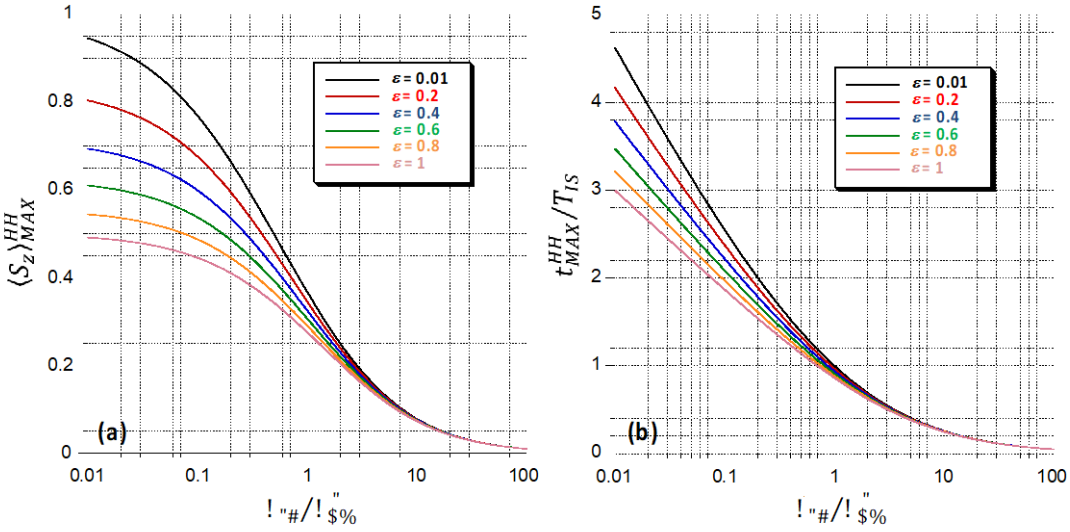

Figure 1 : *I-S* model calculations for HHCP with $\lambda_S = T_{IS}/T_{1\rho}^{S} = 0$. (a) Maximum value of *S* spin polarization $\langle S_z \rangle_{MAX}^{HH}$ (Eq. (A.8)) and (b) time ratio of maximum t_{MAX}^{HH}/T_{IS} (Eq. (A.9)) as a function of $\lambda_I = T_{IS}/T_{1\rho}^{I}$ for several values of heat capacity ratio ε.

Fig. 2

Raya et al

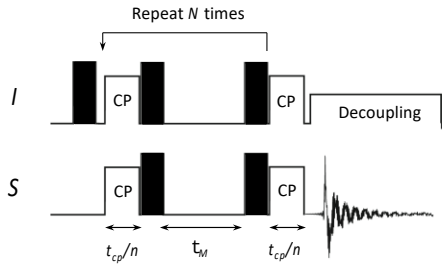

Figure 2 : Schematic representation of the pulse sequence for Multiple-Contact Cross-polarization (MC-CP). The filled rectangles indicate $\pi/2$ pulses.

Fig. 3

Raya et al

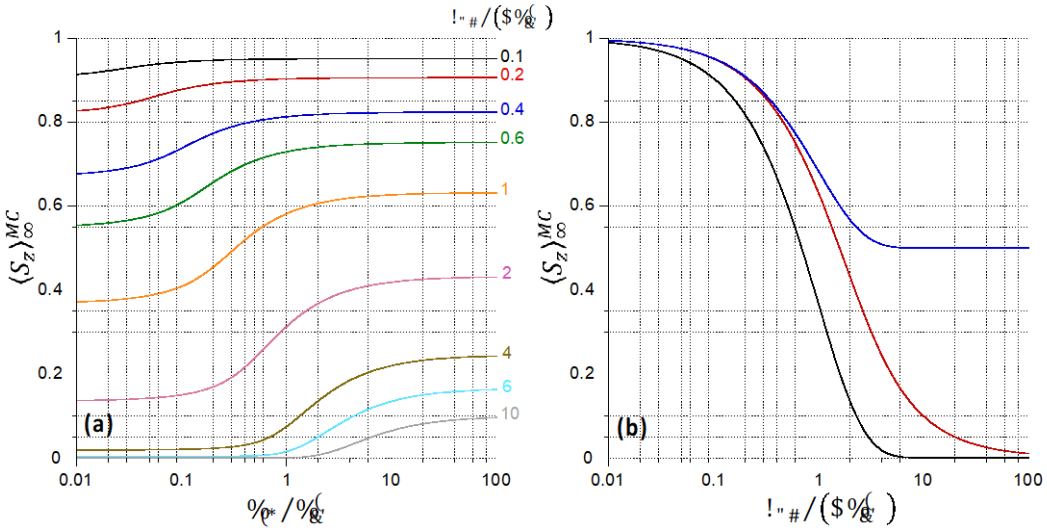

Figure 3 : *I-S* model calculations for MC-CP with $\varepsilon = 0$ and $\lambda_S = 0$. Amplitude of the build-up curve $\langle S_z \rangle_\infty^{MC}$: (a) versus $\lambda_I = T_{IS}/T_{1\rho}^I$ for several values of $t_{CP}/\left(nT_{1\rho}^I\right)$; (b) versus $t_{CP}/\left(nT_{1\rho}^I\right)$ with $\lambda_I \ll 1$ (black line) (Eq. (7)) and with $\lambda_I \gg 1$ (red line) (Eq. (8)). The blue line is the amplitude ratio $\langle S_z \rangle_\infty^{MC(2)}/\langle S_z \rangle_\infty^{MC(1)}$ with $\lambda_I \gg 1$ when doubling the length of the CP steps from experiment (1) to experiment (2) ($n^{(2)} = n^{(1)}/2$).

Fig. 4

Raya et al

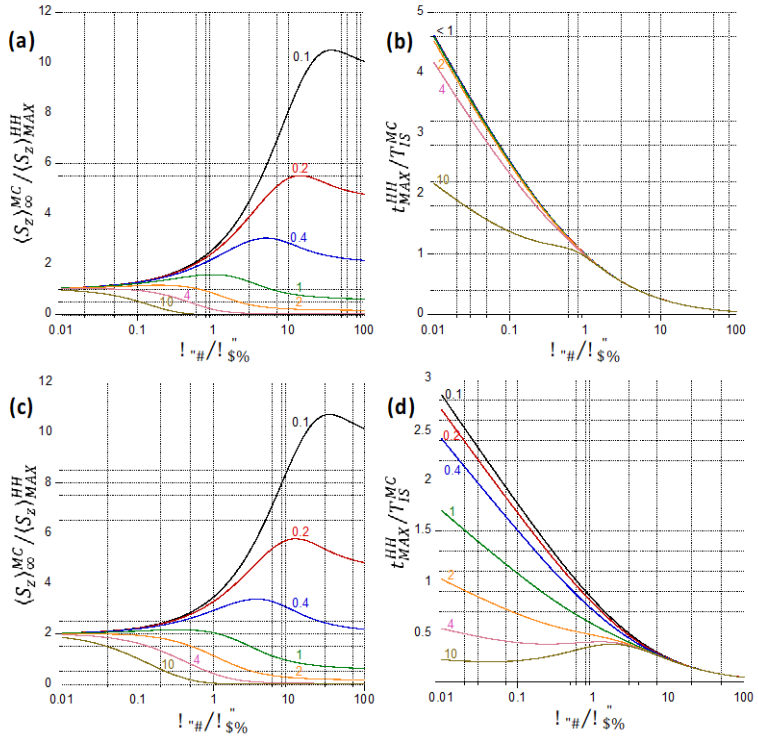

Figure 4 : *I-S* model calculations for HHCP and MC-CP with $\lambda_S = 0$. (a and c) Amplitude and (b and d) time ratios, $r_S = \langle S_z \rangle_\infty^{MC} / \langle S_z \rangle_{MAX}^{HH}$ and $r_T = t_{MAX}^{HH} / T_{IS}^{MC}$, as a function of $\lambda_I = T_{IS}/T_{1\rho}^I$ for several values of $t_{CP}/(nT_{IS})$: (a and b) $\varepsilon = 0.01$; (c and d) $\varepsilon = 1$.

Fig. 5
Raya et al

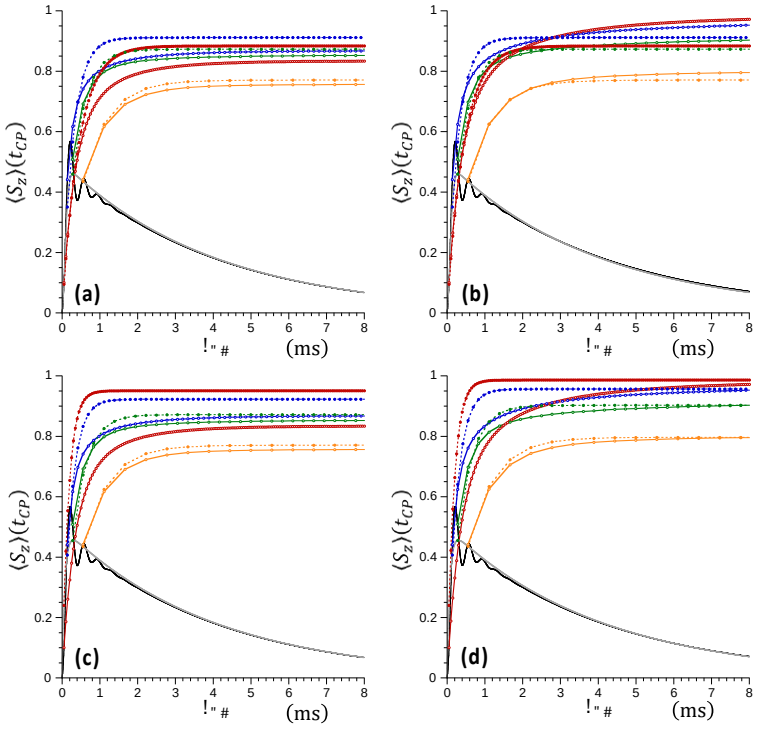

Figure 5 : *I-S* and *I-I*-S* model calculations for HHCP and MC-CP. Polarization evolution of *S*-spin magnetization $\langle S_z \rangle (t)$ as a function of the total contact time t_{CP} for a MAS powder : Numerical integration (black solid line for HHCP and colored open circles/solid lines for MC-CP) of the *I-I*-S* model QM master equation (Eq. (B.1)) versus analytical solutions (grey solid line for HHCP and colored full circles/dotted lines for MC-CP) obtained by (a and b) the AW approximation (Eqs (B.28) and (B.31))) or (c and d) the *I-S* model (Eqs (A.7) and (A.14)) ; MC-CP with $t_{CP}/n = 50$ µs (red), $t_{CP}/n = 138.8$ µs (blue), $t_{CP}/n = 277.5$ µs (green), $t_{CP}/n = 555$ µs (orange) ; (a and c) $T_{1\rho}^{I} = T_{1\rho}^{S} = 4$ ms ; (b and d) $T_{1\rho}^{I} = 2$ ms and $1/T_{1\rho}^{S} = 0$. The other parameters are $|\Delta|/2\pi = \omega_r/2\pi = 15$ kHz, $n_I = 1$, $1/\sqrt{M_2^{IS}} = 45$ µs and $T_{dp} = 0.2$ ms ($S^2 = 1$ or $1/\tau_c = 0$) for the *I-I*-S* model ; $T_{IS} = 0.15$ ms and $\varepsilon = 1$ for the *I-S* model.

Fig. 6

Raya et al

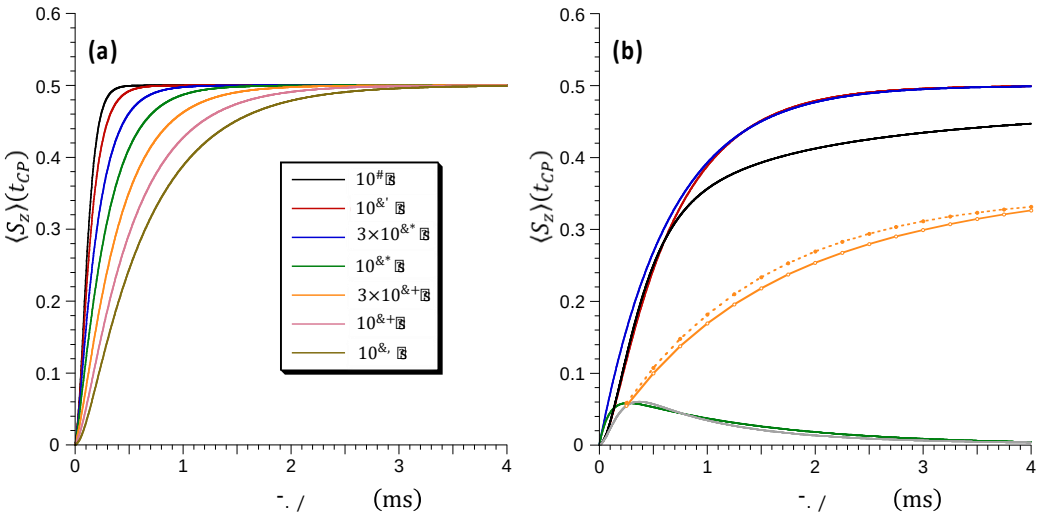

Figure 6 : *I-S* and *I-I*-S* model calculations for HHCP and MC-CP with $t_{CP}/n = 250$ µs $(1/T_{1\rho}^{S} = 0)$. Polarization evolution of *S*-spin magnetization $\langle S_z \rangle(t)$ as a function of the total contact time t_{CP} for a MAS powder : (a) HHCP dynamics calculated by using the *I-I*-S* model in the AW approximation for several values of τ_c with $1/T_{1\rho}^{I} = 0$; (b) Numerical integration (black solid line for HHCP with $1/T_{1\rho}^{I} = 0$, grey solid line for HHCP with $T_{1\rho}^{I} = 0.1$ ms and orange open circles/solid lines for MC-CP with $T_{1\rho}^{I} = 0.1$ ms) of the *I-I*-S* model QM master equation (Eq. (B.1)) versus the analytical solutions obtained by the AW approximation (Eqs (B.28) and (B.31))) (red solid line for HHCP with $1/T_{1\rho}^{I} = 0$) or the *I-S* model (Eqs (A.7) and (A.14)) (blue solid line for HHCP with $1/T_{1\rho}^{I} = 0$, green solid line for HHCP with $T_{1\rho}^{I} = 0.1$ ms and orange full circles/dotted lines for MC-CP with $T_{1\rho}^{I} = 0.1$ ms). The other parameters are $|\Delta|/2\pi = \omega_r/2\pi = 15$ kHz, $n_I = 1$, $1/\sqrt{M_2^{IS}} = 45$ µs, $T_{dp} = 0.1$ ms and $S^2 = 0.1$ for the *I-I*-S* model ; $T_{IS} = 1.3$ ms and $\varepsilon = 1$ for the *I-S* model.

Fig. 7

Raya et al

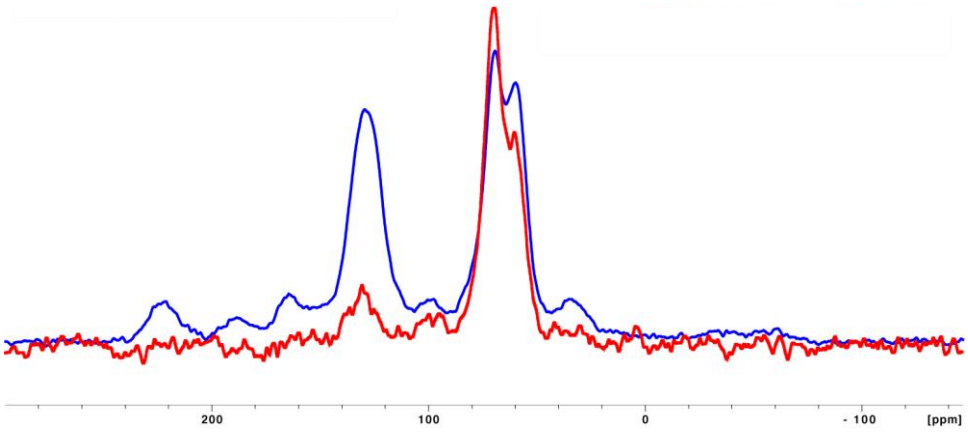

Figure 7 : ^{13}C NMR MAS single pulse excitation (SPE) (blue line) and HHCP with $t_{CP} = 555$ µs (red line) spectra of GO. MAS rate $\nu_r = 18$ kHz ; measuring time : 17 h (SPE) and 2 h (HHCP).

Fig. 8
Raya et al

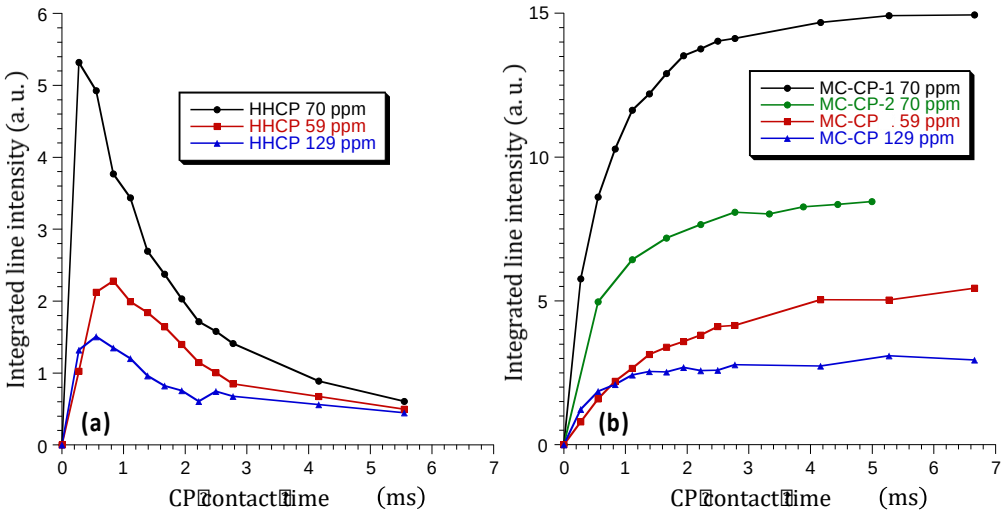

Figure 8 : Time dependence of ^{13}C magnetization for the C-OH (black or green circles), C-O-C (red squares) and C=C (blue triangles) sites of GO in the ^{1}H-^{13}C (a) HHCP and (b) MC-CP experiments with $\tau_M = 50$ ms and $t_{CP}/n = 277.5$ µs. In the case of the C-OH resonance (70 ppm), both the MC-CP data with $t_{CP}/n = 277.5$ µs (black circles) and 555 µs (green circles) are reported. The peak intensities were obtained by deconvolution of the ^{13}C NMR MAS spectra with the solid line shape analysis (SOLA) package as implemented in the BRUKER™ TopSpin 4.0.8 software.

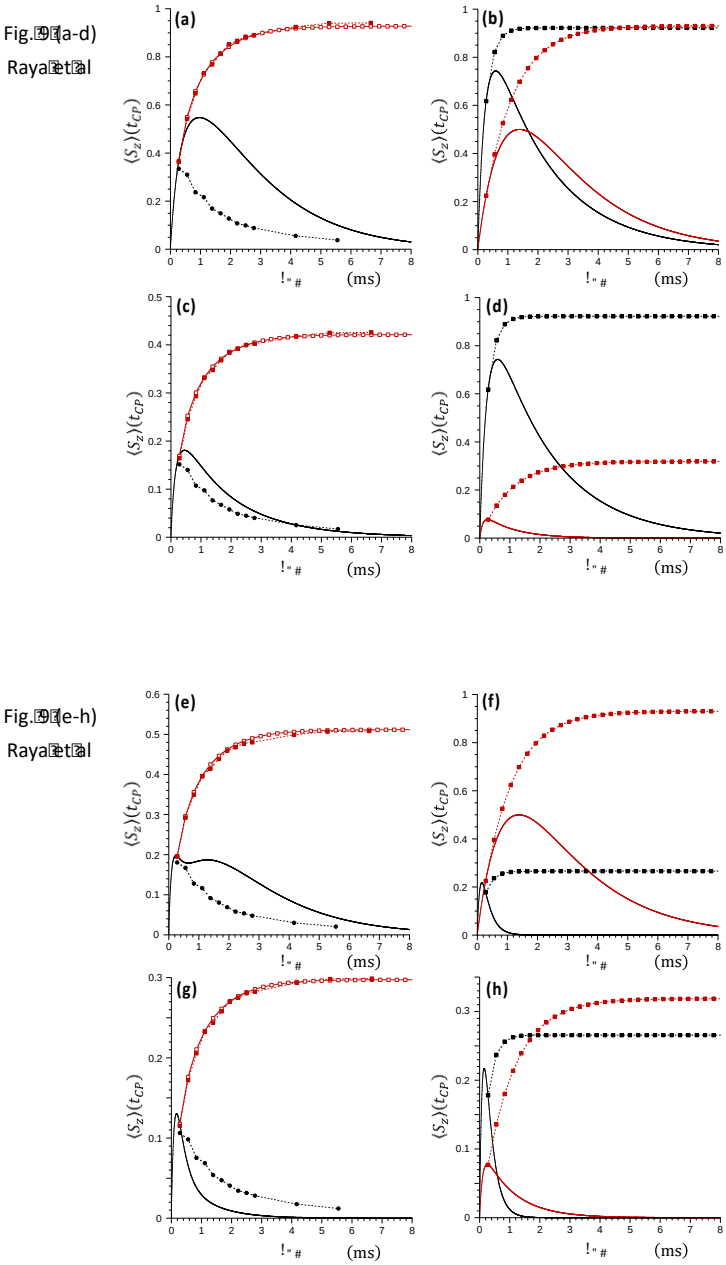

Figure 9 : Experimental and calculated (*I-S* model with $\varepsilon = 0$ and $\lambda_S = 0$) ^{1}H-^{13}C CPMAS dynamics for the C-OH resonance (70 ppm) of GO : (a, c, e, and g) HHCP (black circles/dotted lines) and MC-CP with $t_{CP}/n = 277.5$ µs (red full squares/dotted lines) experimental intensities versus two-component calculations (black solid line for HHCP and red open squares/solid lines for MC-CP) ; (b, d, f, and h) corresponding individual components (1) and (2) represented by : black (1) and red (2) solid lines for HHCP ; black (1) and red (2) full squares/dotted lines for MC-CP. The cross-relaxation time constants are $T_{CH}^{(1)} = 0.25$ ms and $T_{CH}^{(2)} = 1$ ms. The ^{1}H spin-lattice relaxation times in the rotating frame (and component weight%) are : (a and b) $T_{1\rho}^{H(1)} = 2$ ms (36%) and $T_{1\rho}^{H(2)} = 2$ ms (64%) ; (c and d) $T_{1\rho}^{H(1)} = 2$ ms (17%) and $T_{1\rho}^{H(2)} = 0.1$ ms (83%) ; (e and f) $T_{1\rho}^{H(1)} = 0.1$ ms (63%) and $T_{1\rho}^{H(2)} = 2$ ms (37%) ; (g and h) $T_{1\rho}^{H(1)} = 0.1$ ms (40%) and $T_{1\rho}^{H(2)} = 0.1$ ms (60%).

Fig. 10

Raya et al

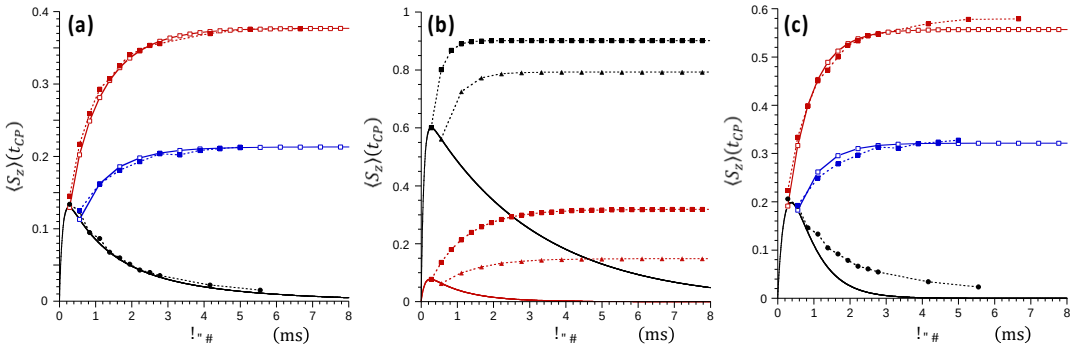

Figure 10 : Experimental and calculated (*I-S* model with $\lambda_S = 0$) ^{1}H-^{13}C CPMAS dynamics for the C-OH resonance (70 ppm) of GO : (a) HHCP (black circles/dotted lines) and MC-CP with $t_{CP}/n = 277.5$ µs (red full squares/dotted lines) and $t_{CP}/n = 555$ µs (blue full squares/dotted lines) experimental intensities versus two-component calculations (black solid line for HHCP and red or blue open squares/solid lines for MC-CP. The cross-relaxation time constants (heat capacity ratio) are $T_{CH}^{(1)} = 0.11$ ms ($\varepsilon^{(1)} = 0.5$) and $T_{CH}^{(2)} = 1$ ms ($\varepsilon^{(2)} = 0$). The ^{1}H spin-lattice relaxation times in the rotating frame (component weight%) are $T_{1\rho}^{H(1)} = 2$ ms (10%) and $T_{1\rho}^{H(2)} = 0.1$ ms (90%) ; (b) corresponding individual components (1) and (2) represented by : black (1) and red (2) solid lines for HHCP ; black (1) and red (2) full squares or triangles/dotted lines for MC-CP ; (c) same as (a) for a single-component calculation with $T_{CH} = 0.66$ ms and $T_{1\rho}^{H} = 0.23$ ms ($\varepsilon = 0$).

Table of contents

Structural and dynamical details are probed by kinetics of ^{1}H-^{13}C single- and multiple-contact cross-polarization in graphene oxide

Graphical Abstract